Calhoun
Institutional Archive of the Naval Postgraduate School

Calhoun: The NPS Institutional Archive

Theses and Dissertations | Thesis Collection

1994-06

A calibration of the Naval Postgraduate School middle ultraviolet spectrograph and an analysis of þÿ t h e O I I 2 4 7 0 © A e m i s s i o n o b t a i n e d b y t ultraviolet spectrograph

Hymas, Hewitt M.

Monterey, California. Naval Postgraduate School

DUDLEY KNOX LIBRARY

Calhoun is a project of the Dudley Knox Library at NPS, furthering the precepts and goals of open government and government transparency. All information contained herein has been approved for release by the NPS Public Affairs Officer.

Dudley Knox Library / Naval Postgraduate School
411 Dyer Road / 1 University Circle
Monterey, California USA 93943

http://www.nps.edu/library

DUDLEY KNOX LIBRARY
NAVAL POSTGRADUATE SCHOOL
MONTEREY CA 93943-5101

Approved for public release; distribution is unlimited

A Calibration of the Naval Postgraduate School Middle Ultraviolet Spectrograph and an Analysis of the OII 2470 Å Emission Obtained by the Middle Ultraviolet Spectrograph

by

Hewitt M. Hymas
Lieutenant, United States Navy
B.S., University of Utah, 1986

Submitted in partial fulfillment of the
requirements for the degree of

MASTER OF SCIENCE IN PHYSICS

from the

NAVAL POSTGRADUATE SCHOOL
June 1994

REPORT DOCUMENTATION PAGE

1a. REPORT SECURITY CLASSIFICATION Unclassifed	1b. RESTRICTIVE MARKINGS
2a. SECURITY CLASSIFICATION AUTHORITY	3. DISTRIBUTION/ AVAILABILITY OF REPORT Approved for public release; distribution is unlimited.
2b. DECLASSIFICATION/DOWNGRADING SCHEDULE	
4. PERFORMING ORGANIZATION REPORT NUMBER(S)	5. MONITORING ORGANIZATION REPORT NUMBER(S)
6a. NAME OF PERFORMING ORGANIZATION Naval Postgraduate School 6b. OFFICE SYMBOL *(If Applicable)* 33	7a. NAME OF MONITORING ORGANIZATION Naval Postgraduate School
6c. ADDRESS *(city, state, and ZIP code)* Monterey, CA 93943-5000	7b. ADDRESS *(city, state, and ZIP code)* Monterey, CA 93943-5000
8a. NAME OF FUNDING/SPONSORING ORGANIZATION 8b. OFFICE SYMBOL *(If Applicable)*	9. PROCUREMENT INSTRUMENT IDENTIFICATION NUMBER
8c. ADDRESS *(city, state, and ZIP code)*	10. SOURCE OF FUNDING NUMBERS PROGRAM ELEMENT NO. / PROJECT NO. / TASK NO. / WORK UNIT ACCESSION NO.

11. TITLE *(Include Security Classification)* A CALIBRATION OF THE NAVAL POSTGRADUATE SCHOOL MIDDLE ULTRAVIOLET SPECTROGRAPH AND AN ANALYSIS OF THE OII 2470 Å EMISSION OBTAINED BY THE MIDDLE ULTRAVIOLET SPECTROGRAPH

12. PERSONAL AUTHOR(S)
Hymas, Hewitt M.

13a. TYPE OF REPORT Master's Thesis	13b. TIME COVERED FROM TO	14. DATE OF REP*(year, month,day)* June, 1994	15. PAGE COUNT 73

16. SUPPLEMENTARY NOTATION
The views expressed in this thesis are those of the author and do not reflect the official policy or position of the Department of Defense or the U.S. Government.

17. COSATI CODES			18. SUBJECT TERMS *(continue on reverse if necessary and identify by block number)*
FIELD	GROUP	SUBGROUP	Spectroscopy, Middle Ultraviolet Spectrograph, Ultraviolet Spectra, Dayglow

19. ABSTRACT *(Continue on reverse if necessary and identify by block number)*

The NPS middle ultraviolet spectrograph, MUSTANG, instrument was tested using standard techniques to determine the wavelength calibration and overall sensitivity. The instrument was launched on March 10, 1994 on a NASA sounding rocket from Poker Flats, Alaska. Post-flight calibration indicates the wavelength calibration did not change as a result of the launch and no significant change in the sensitivity calibration. Ultraviolet dayglow spectra of the earth's ionosphere from 1800 Å to 3400 Å were obtained during a similar launch on March 19,1992 from White Sands Missile Range, New Mexico. Data were obtained on the downleg of this earlier experiment and range in altitude from 115 km to 320 km. Analysis of the data from 2420 Å to 2490 Å was conducted to obtain the intensity profile of the OII 2470 Å multiplet. The analysis used synthetic spectra generated for the N2 Vegard-Kaplan and the nitric-oxide gamma band emissions.

20. DISTRIBUTION/AVAILABILITY OF ABSTRACT [X] UNCLASSIFIED/UNLIMITED [ ] SAME AS RPT. [ ] DTIC USERS	21. ABSTRACT SECURITY CLASSIFICATION Unclassified
22a. NAME OF RESPONSIBLE INDIVIDUAL David D. Cleary	22b. TELEPHONE (Include Area Code) (408) 656-2828 / 22c. OFFICE SYMBOL Code PH/CL

DD FORM 1473, 84 MAR 83 APR edition may be used until exhausted SECURITY CLASSIFICATION OF THIS PAGE
All other editions are obsolete Unclassified

ABSTRACT

The MUSTANG, NPS middle ultraviolet spectrograph, instrument was tested using standard techniques to determine the wavelength calibration and overall sensitivity. The instrument was launched on March 10, 1994 on a NASA sounding rocket from Poker Flats, Alaska. Post-flight calibration indicates the wavelength calibration did not change as a result of the launch and no significant change in the sensitivity calibration. Ultraviolet dayglow spectra of the earth's Ionosphere from 1800 Å to 3400 Å were obtained during a similar launch on March 19, 1992 from White Sands Missile Range, New Mexico. Data were obtained on the downleg of this earlier experiment and range in altitude from 115 km to 320 km. Analysis of the data from 2420 Å to 2490 Å was conducted to obtain the intensity profile of the OII 2470.4 Å multiplet. The analysis used synthetic spectra generated for the N_2 Vegard-Kaplan and the nitric-oxide gamma band emissions.

Thesis
H976s
c.1

TABLE OF CONTENTS

DUDLEY KNOX LIBRARY
NAVAL POSTGRADUATE SCHOOL
MONTEREY CA 93943-5101

I. INTRODUCTION

The variability of the ionospheric electron density needs to be better understood because it strongly influences high frequency (HF) radio communications, over-the-horizon (OTH) radar, ballistic missile early warning systems, and the Ground Wave Emergency Network (GWEN). In addition to this, the Joint Chiefs of Staff have prioritized the measurement of the ionospheric electron density as number five of 50 critical global parameters for inclusion in a defense environmental satellite (MJCS 154-86 dated March 21, 1986).

The ionosphere has the ability to reflect transmitted radio waves. The altitude at which these radio waves reflect is dependent on the electron density of the ionosphere and the wavelength of the transmitted radio wave. This atmospheric 'mirror' is not completely smooth, but has many imperfections. Because of these imperfections and their effect on radio communication and radar it is important to be able to measure the electron density profile and how this profile varies over the entire globe. Currently, measurement of the ionospheric electron density is limited to 20 ground-based ionosonde stations scattered throughout the world. Although this is accurate locally, this method is not

capable of being used on a global basis. What is needed is a low-power orbiting system capable of passively measuring the electron density.

Joint NPS/NRL research is currently testing the Middle Ultraviolet Spectrograph (MUSTANG) and the High Resolution Airglow and Aurora Spectrograph (HIRAAS) for this purpose. By measuring the intensity of atmospheric emissions, the ion densities may be determined. The electron density may then be inferred from the ion density. MUSTANG was first launched aboard a NASA sounding rocket in March of 1990 from the White Sands Missile Range, New Mexico, and again in a similar launch in March of 1992. Analysis of the data obtained from the downleg of the March 1992 launch is the topic of this thesis.

A. THESIS OBJECTIVES

This thesis has two main goals; calibration of the MUSTANG instrument for the March, 1994 launch from Poker Flats, Alaska and the determination of the intensity profile for the OII 2470 Å multiplet from data obtained from the March 19, 1992 launch from White Sands Missile Range, New Mexico. Accurate calibration of the instrument prior to launch is critical for analyzing the data obtained during the rocket flight. The ultraviolet dayglow spectra used to determine the intensity profile were obtained on the down leg of the 1992 flight and range from 115 km to 320 km.

B. THESIS OUTLINE

This thesis is divided into six Chapters and one Appendix. A brief introduction of the ionosphere along with the objectives of this thesis are given in Chapter I. Chapter II discusses the ionosphere in greater detail and briefly introduces atomic and molecular emissions. Chapter III describes the instrument in detail and the procedure for collecting the data. Chapter IV develops the method and theory of the MUSTANG calibration and contains the final calibration results. Chapter V describes the use of synthetic spectra and the method used in analyzing the OII 2470 Å emission. Finally, Chapter VI concludes with a summary of the results.

II. BACKGROUND

A. THE IONOSPHERE

The depth of penetration of solar radiation incident on the earth's atmosphere is dependent on wavelength. Figure 1 shows the altitude of unit optical depth for radiation with wavelengths up to 3500 Å and the atmospheric constituent mainly responsible for its absorption. Also noted are the ionization limits for N_2, N, NO, O, and O_2. Unit optical depth is the altitude where the incoming radiation intensity is decreased by 1/e and is important because this is where most of the energy is deposited. Radiation with wavelengths longer than approximately 3100 Å penetrates to the surface of the earth. Radiation from approximately 1340 Å to 3100 Å does not reach the surface of the earth, but instead dissociates O_2 and ozone (O_3). Radiation with wavelengths shorter than approximately 1340 Å penetrates to different altitudes, depending on wavelength, before ionizing the different atmospheric constituents. Notice the ionization limits for all the major atmospheric constituents are included in this range of wavelengths. This ionizing of the atmosphere is the creation of the ionosphere.

The ionosphere begins about 50 km and extends up to about 1000 km. It is primarily created by atmospheric constituents being ionized by incoming solar radiation with

wavelengths less than 1340 Å. The ionization rate in the ionosphere is proportional to the photon flux multiplied by the number density. Figure 2 shows schematically how the electron production rate follows the photon flux and particle number density curves. At high altitudes there is an abundance of photons, but few particles. The reverse is true for low altitudes, there is an abundance of particles, but few photons; most having been absorbed at higher altitudes. This resulting ionization curve is referred to as *Chapman Profile*. Figure 3 is a more realistic view of the ionosphere electron density profile along with the atmospheric constituents contributing to that density.

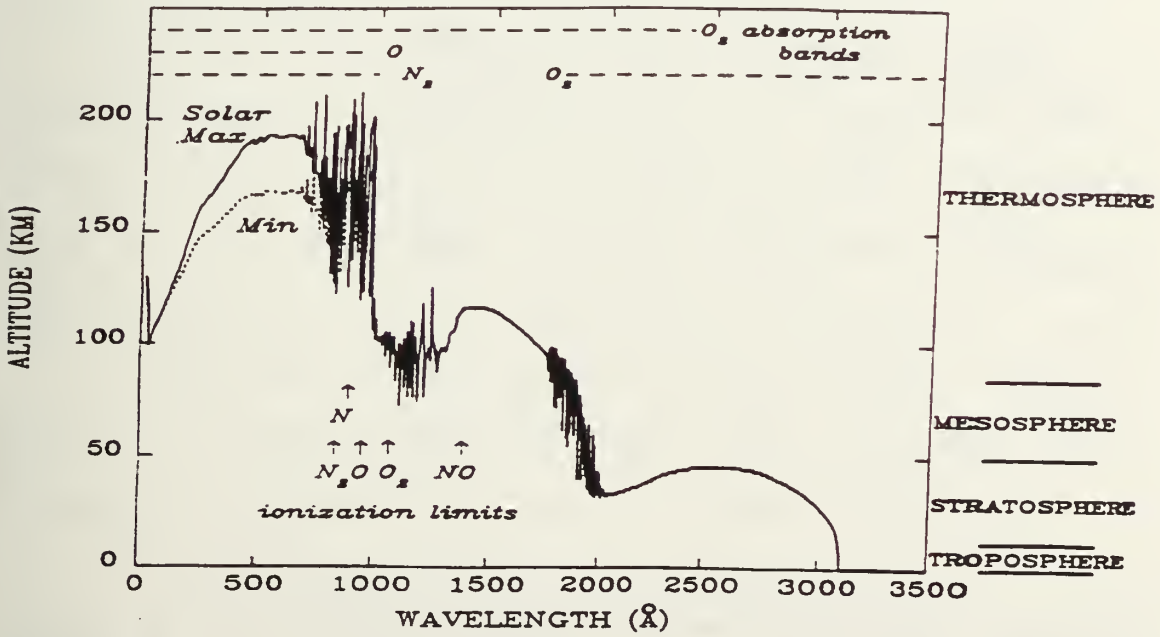

Figure 1: Unit optical depth for each wavelength.

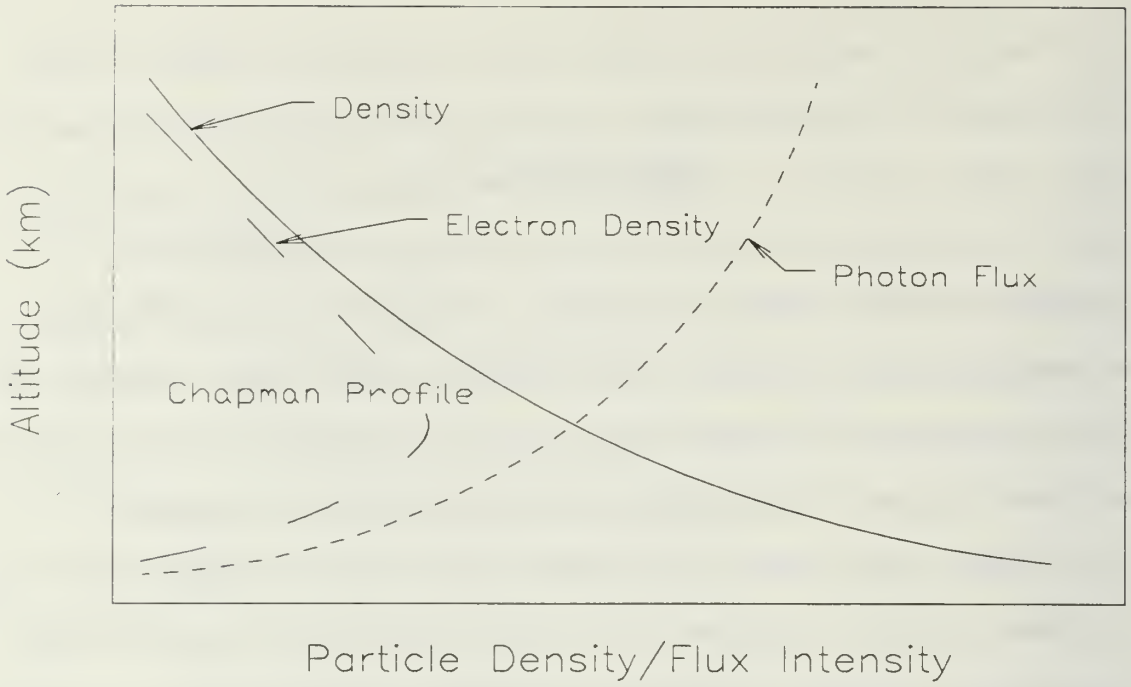

Figure 2: Electron production curve.

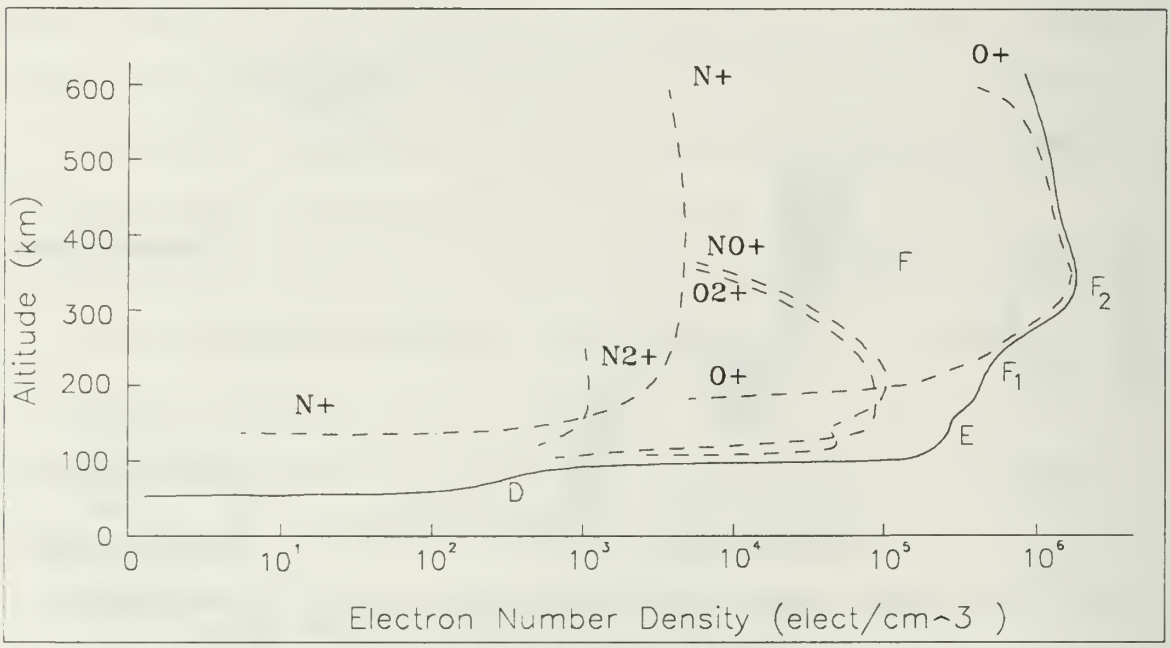

Figure 3: Ionosphere electron density profile. The solid line is electron density and the dashed lines are ion densities.

The ionosphere is comprised of four layers: D, E, F_1 and F_2. The electron density and altitude of each layer depends primarily on the intensity of incoming solar radiation. The D-region extends from 50 km to 90 km. This is the lowest region of the ionosphere and is created mainly by short wavelength ultraviolet and x-rays with the maximum electron density occurring about 75 to 80 km. This layer is very weakly ionized with elecron densities on the order of 10^2 - 10^4 electrons per cubic centimeter. At night, with no incident radiation, the electrons and ions recombine and the D layer disappears. In D, E, and F1 layer the primary loss mechanism is dissociative recombination, for example $NO^+ + e^- \rightarrow N + O$. The major ion in the D layer is NO^+.

The E layer lies between 90 and 140 km with higher electron densities ranging from 10^4 to 10^5 elec/cm^3. The electron density in this layer weakens at night, but this layer is still capable of reflecting radio waves back to earth. The major ions in this layer are NO^+ and O_2^+.

The F1 layer lies between 140 and 200 km with electron densities slightly higher than the E layer. The major ions in this layer are NO^+, O_2^+, and to a lesser extent O^+.

The F2 layer extends from 200 km and beyond. In this region O^+ is the major positive ion. The electron density profile peaks in this region with densities on the order of $2x10^6$ elec/cm^3. This peak is formed from O^+ diffusing downward to approximately 250 km where it is chemically lost

and the density begins to decrease. The primary loss mechanism is $O^+ + m \rightarrow O + m^+$, where m is NO or O_2. The electron density in this layer decreases by about a factor of three at night, but this layer does not disappear. The atmospheric density is so low at these altitudes that it requires more than one night for the ions and electrons to recombine. The downward diffusion of O^+ also plays a role in maintaining this layer at night.

As mentioned in the Introduction, the ability to measure these electron densities is important because of the profound effect they have on communications and radars.

B. ATOMIC AND MOLECULAR EMISSIONS

Atoms and molecules can exist in many discrete energy states and often jump from one energy state to another. Although a transition from a higher energy state to a lower energy state may occur spontaneously, a transition from lower energy to higher energy may not. Some mechanism capable of transferring energy to the atom or molecule is required. There are many mechanisms capable of transferring energy, but this study is primarily concerned with only two:

1. Absorption of an incident photon, or photoexcitation;
2. Collisional excitation with an incident photo-electron.

Absorption of incoming solar radiation will excite atmospheric atoms and molecules to higher energy states. If

this incident radiation is sufficiently energetic, it will ionize the atom or molecule and create a photo-electron. These photo-electrons can excite other atoms and molecules through collisional excitation. These excited atoms and molecules remain in higher energy states for a short period of time before returning to the ground state. When this transition occurs a photon with an energy equal to the change in energy is emitted. The important point being that each species of atoms or molecules can only transition between discrete energy states. Measuring the energy of the emitted photon can then be used to determine which species it originated from. Since wavelength is much easier to measure than energy, the relationship $E = \frac{hc}{\lambda}$ provides the link required. The MUSTANG instrument was designed to measure intensity versus wavelength.

In the case of the atom, these transitions primarily involve a change of state of the outer orbiting electrons. For molecules, the situation is slightly different. Molecules can also rotate and vibrate about a central axis. In addition to electronic transitions, a molecule will also have vibrational and rotational transitions. A typical energy level diagram is shown in Figure 4. As seen in the figure, for any given electronic transition there are many possible vibrational transitions, and for any vibration transition there are many possible rotational transitions. The typical energies for these transitions are:

1. Electronic, 10 eV;

2. Vibrational, .1 eV;

3. Rotational, .001 eV.

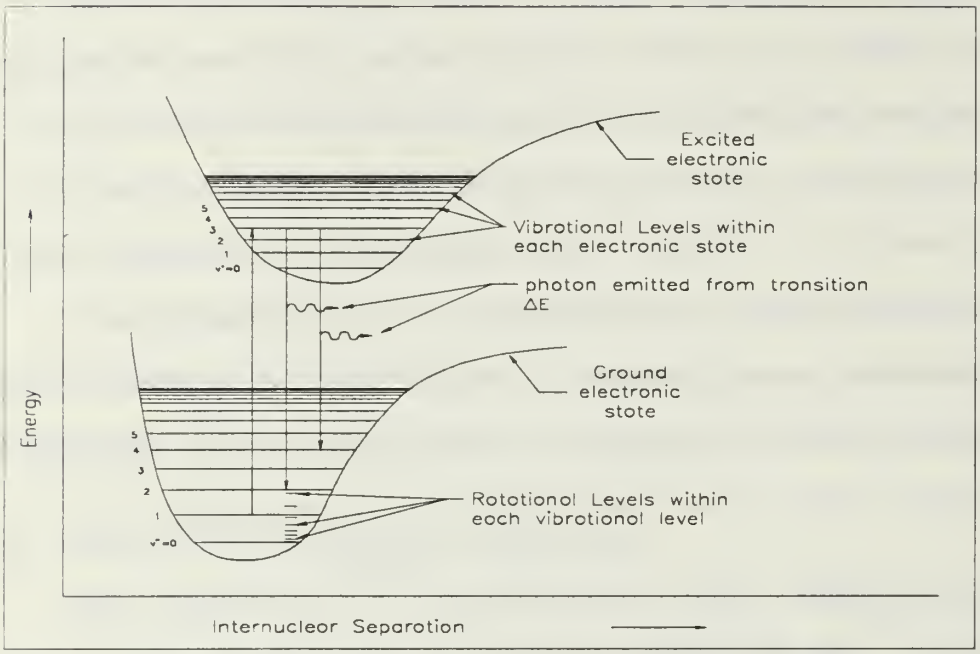

Figure 4: Molecular energy level transition diagram.

III. THE EXPERIMENT

A. INTRODUCTION

Previous work suggests that ion densities may be determined through measurement of emissions from neutral constituents (Bosserman, 1989 and Danczyk, 1989). The ionospheric electron density can then be inferred from the ion densities. To test this theory NPS' MUSTANG and NRL's HIRASS were launched on a NASA sounding rocket in March 1990 and again in March 1992. During each flight a door on the payload section opened at approximately 100 km exposing the two instruments to the atmosphere. After outgassing the attitude control system maneuvered the payload to the specified instrument observation-zenith-angle (OZA). For the 1992 launch the OZA for the upleg was 100 degrees. Data were taken from 150 km to 320 km. At apogee the payload was again maneuvered so the OZA was 90 degrees. Data were taken on the downleg from 320 km to 115 km.

B. INSTRUMENT DESCRIPTION

The MUSTANG instrument is a 1/8th meter Ebert-Fastie spectrograph with a 1/8th meter telescope and a wavelength coverage from 1800 Å to 3400 Å. This wavelength coverage is the middle ultraviolet (MUV) and part of the near

ultraviolet (NUV) portion of the electromagnetic spectrum. A schematic diagram of the instrument is shown in Figure 5.

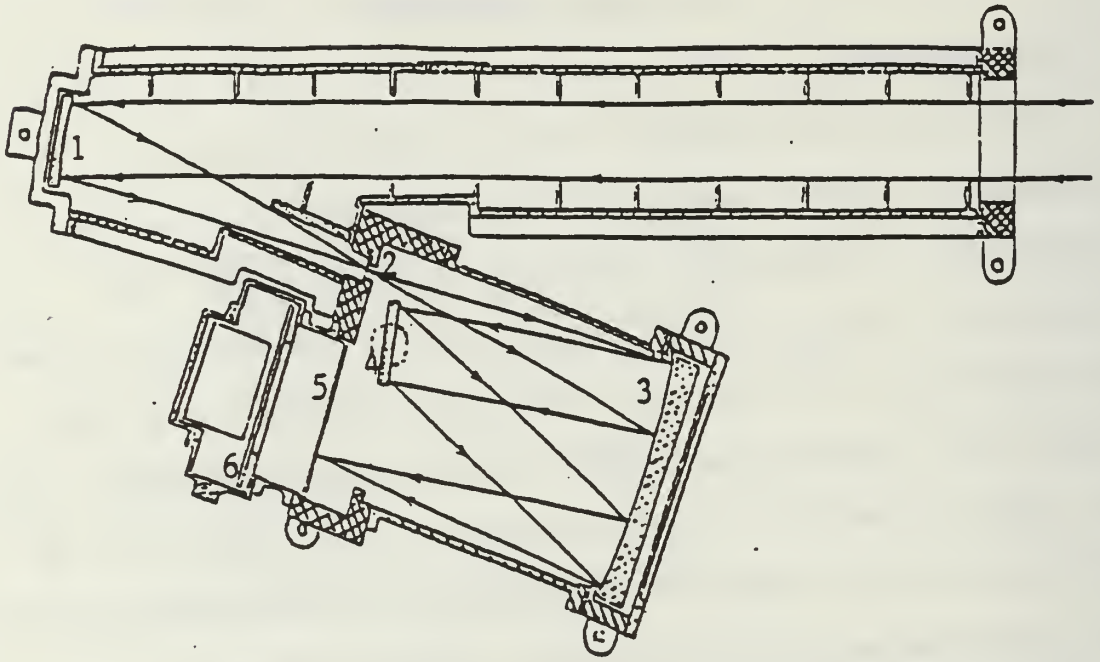

Figure 5: Mustang schematic diagram. The major components shown are: 1) 1/8th m telescope mirror, 2) Spectrograph entrance slit, 3) 1/8th m Ebert mirror, 4) Diffraction grating, 5) ITT image intensifier, 6) Hamamatsu image detector.

Light which enters the telescope is collimated by a series of baffles prior to reaching the telescope mirror. This light is then collected by a 1/8th meter spherical mirror and focused onto a 5mm by 140 um vertical slit. After passing through the entrance slit the light strikes the Ebert mirror. This mirror collimates the light and directs it onto a reflective diffraction grating with a ruling density of 1200 lines/mm. The grating reflects the

collimated light back to the Ebert mirror where it is then focused onto the image intensifier at the spectrograph focal plane.

The image intensifier consists of a quartz input window, a cesium telluride (CsTe) photo-cathode, two micro channel plates (MCP) in cascade, an aluminum screen coated with phosphor, and a fiber optic window. The purpose of the image intensifier is to convert the ultraviolet photons to visible photons with enough gain so they can be detected by the image sensor. This is accomplished when ultraviolet photons at the exit focal plane of the spectrograph strike the photo-cathode generating photo-electrons. These electrons are then accelerated toward the micro channel plates by an accelerating voltage of approximately 200 Volts. The voltage across the micro channel plates is 2000 Volts. The photo-electrons strike the walls of the MCP causing an electron avalanche. This results in approximately 40,000 electrons being produced for every one emitted by the photo-cathode. These electrons are again accelerated by 6000 Volts between the MCP output and the phosphor screen. The screen fluoresces as a result of the incoming electrons. This visible light is transmitted through a fiber optic window with the same spatial configuration as the original spectrum incident on the photo-cathode.

The photodiodes of the Hamamatsu S2300-512F Plasma-Coupled Device (PCD) Linear Image Sensor are sensitive to

light in the 4000 Å to 10000 Å region. Photons emitted from the image intensifier phosphor screen are sensed by the PCD image sensor. The output window of the image intensifier and the PCD image sensor window are both made of a fiber optic material and are placed in physical contact.

The light sensitive section of the image sensor is a 25mm by 5mm photosensitive area consisting of 512 photodiodes arranged in a linear array. The photodiodes are 36um wide, 5mm tall, with a spacing of 50um between the centers of each photodiode. The photodiodes convert the optical energy of incident photons to a charge which is proportional to the corresponding light intensity. The shift register transfers this accumulated charge from the photodiodes to the output with one complete spectrum of 512 voltages in series transmitted every 51.2 ms. This charge then undergoes a 10-bit analog-to-digital conversion and is displayed on the computer or transmitted via rocket telemetry.

IV. CALIBRATION

A. WAVELENGTH CALIBRATION

The wavelength response was the first instrument calibration to be performed. This calibration is required to precisely determine what wavelength each pixel is sensing. The wavelength calibration was accomplished using two sources with well known emissions. The first source was a platinum hollow cathode lamp. This source was chosen because it had 23 useful spectral emissions in the 1800 Å to 3400 Å wavelength range. This lamp was used in conjunction with a Harrison 6522A DC power supply. The lamp was placed on the optical table with the power supply voltage set at 400 Volts and the current at 0 mA. The current was then gradually increased to 15 mA. The average of 25 spectra were taken using 'Labview' and the ground support equipment. This average is shown in Figure 6. The 23 emissions were individually isolated and the centroid of each pixel position was estimated.

After MUSTANG was returned from integration testing, a 'hot spot' was observed on the detector. With no input to the instrument and the high voltage on, an abnormally high output appeared as shown in Figure 7. The source of this is still unknown. This abnormal output was coming from pixels 134-138 as shown in Figure 8. Because of this, the platinum

lamp emission at 2289.27 Å could not be used as it had been in previous calibrations. This output continued to appear throughout the remainder of the calibration, but did not significantly affect the accuracy.

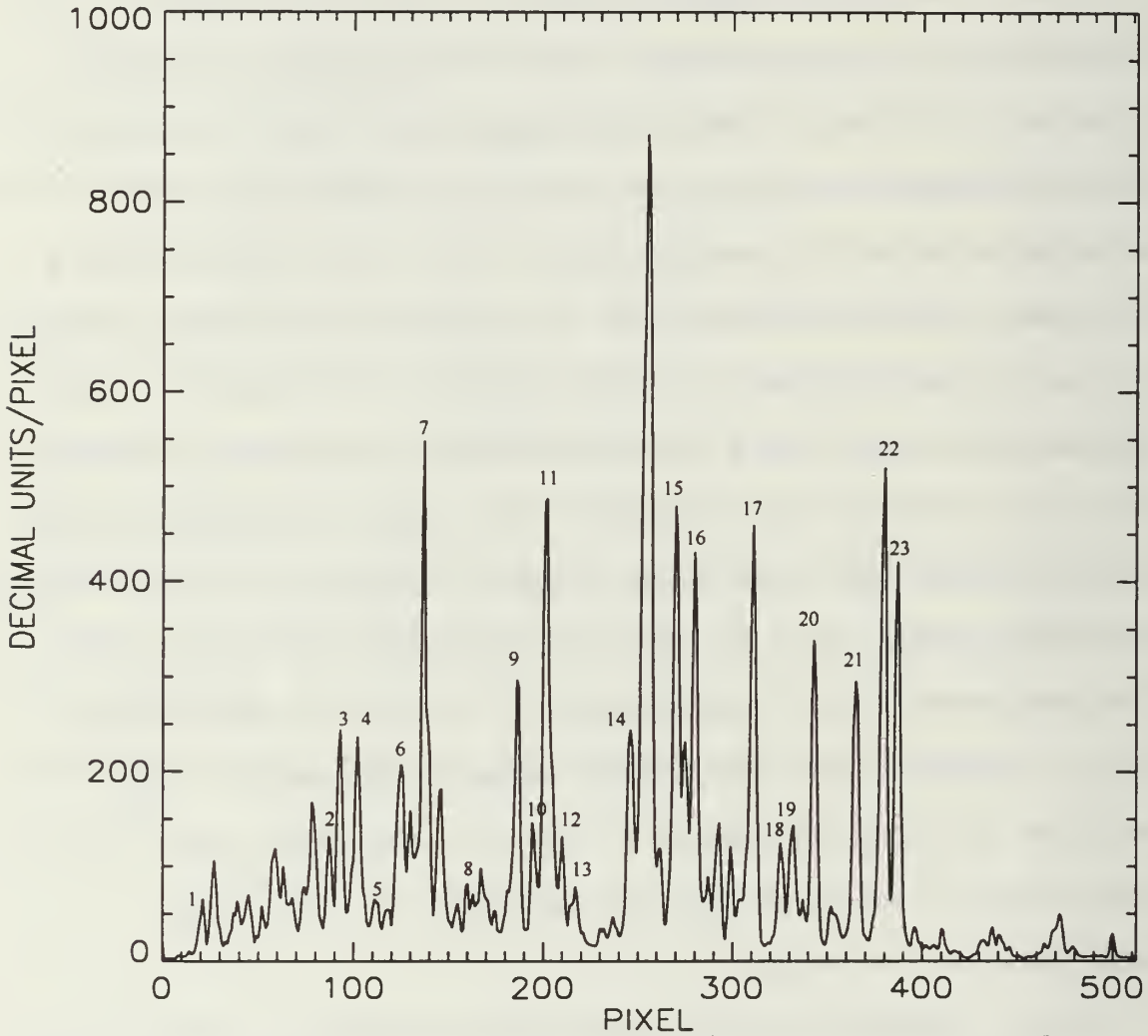

Figure 6: Mustang spectrum from Platinum hollow cathode lamp. The 23 emissions used are identified (see Table I).

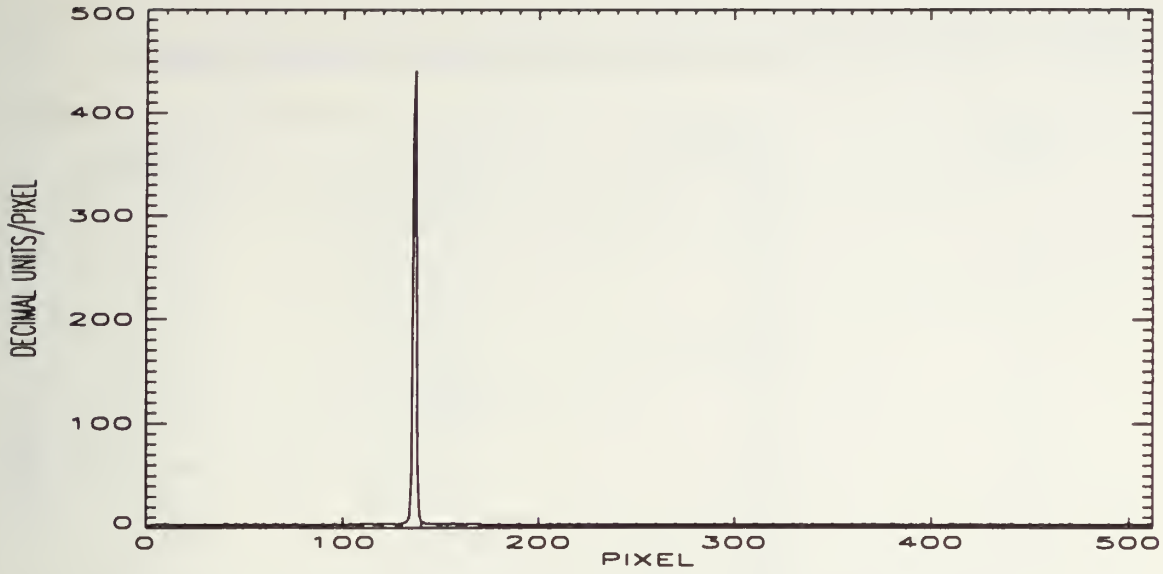

Figure 7: 'Hot spot' with high voltage on.

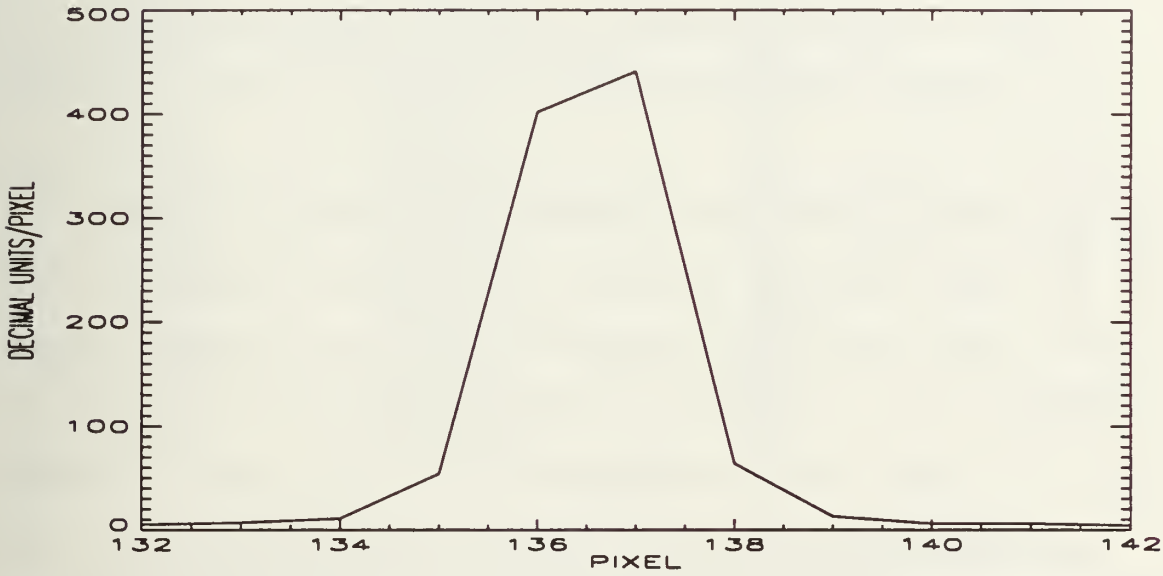

Figure 8: Enlarged view of 'hot spot'.

The same procedure was followed for the second source, which was a mercury lamp. This source was chosen because it added several emissions in the longer wavelength range and one in the shorter wavelength of the detector. The results of this calibration are shown in Table I.

TABLE I. EMISSIONS USED FOR WAVELENGTH CALIBRATION

POINT	SOURCE	λ (Å)	PIXEL
1	Pt	1916.08	21.0
2	Pt	2128.61	87.5
3	Pt	2144.23	92.3
4	Pt	2174.67	101.6
5	Pt	2202.22	111.0
6	Pt	2245.52	125.0
7	Pt	2289.27	137.0
8	Pt	2357.10	159.6
9	Pt	2440.06	185.5
10	Pt	2467.44	195.0
11	Pt	2487.17	201.4
12	Pt	2515.58	210.0
13	Pt	2539.20	217.6
14	Pt	2628.03	246.0
15	Pt	2702.40	270.0
16	Pt	2733.96	280.0
17	Pt	2830.30	310.6
18	Pt	2877.52	325.4
19	Pt	2893.86	331.3
20	Pt	2929.79	343.2
21	Pt	2997.97	365.0
22	Pt	3042.64	379.4
23	Pt	3064.71	386.7
1	Hg	1942.27	29.0
2	Hg	2536.52	216.4
3	Hg	2653.69	254.0
4	Hg	2967.28	355.5
5	Hg	3341.48	477.0

The wavelengths were then plotted versus the pixel position and using the IDL function Poly_fit, a second degree polynomial was fit to the data with the following equation:

$$\lambda = -1.513x10^{-4} X^2 + 3.1996X + 1850.17 \text{ Å} \qquad (4\text{-}1)$$

where X is the pixel number. This is shown in Figure 9.

This equation may now be used to determine the wavelength associated with each pixel.

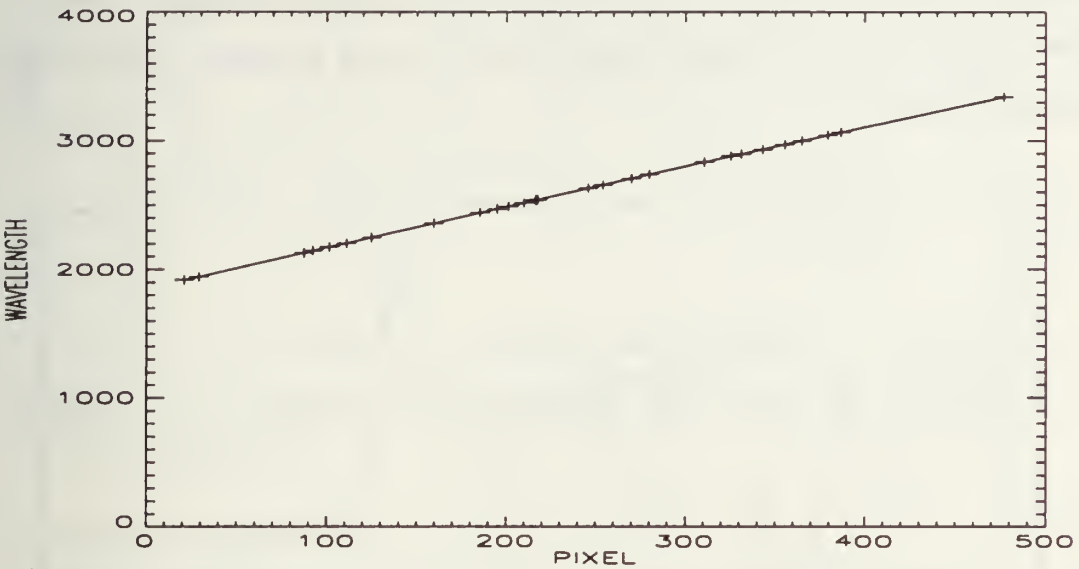

Figure 9: Plot of actual and calculated wavelengths.

Finally, to test the accuracy of the calculated equation the difference between the calculated emission value and the actual emission value was calculated using the pixel values in Table I. The result is shown in Figure 10. The difference between actual and calculated appears to be random with only two points varying more than 2 Å. With the wavelength difference between each pixel being 3.133 Å, the calculated equation is quite accurate.

A second degree polynomial was used to fit the line because it produced the best fit. The difference between a linear fit and the actual data is shown in Figure 11 and has fluctuations about the zero point up to -8 Å. Clearly, the second degree polynomial yields a better fit. A third and

fourth degree polynomial were also fit to the data. The difference between the third degree fit and the actual data is shown in Figure 12. As can be seen in the figure, there was no significant improvement for a third degree or greater polynomial fit.

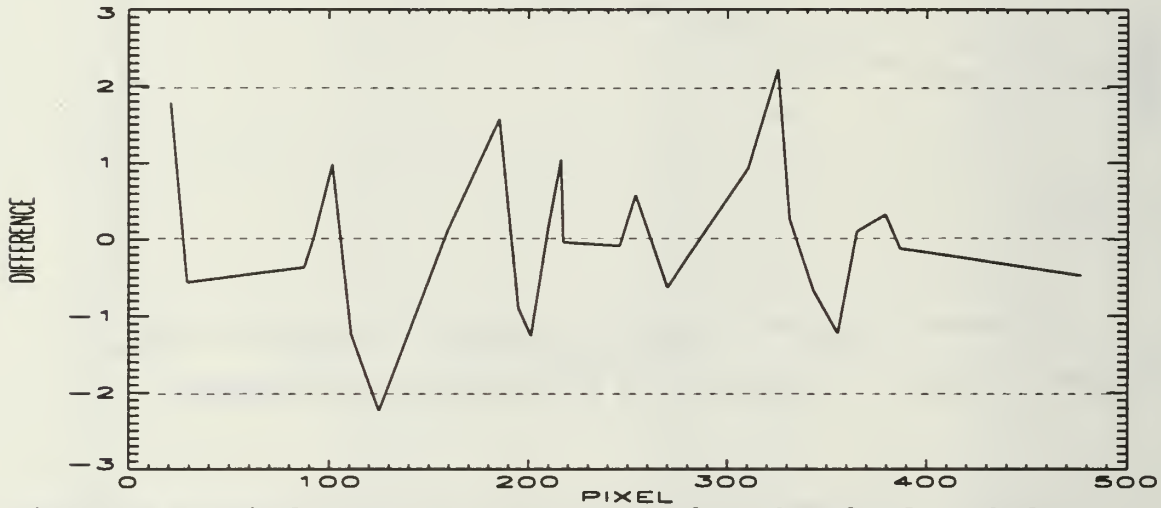

Figure 10: Difference between actual and calculated for a second degree fit.

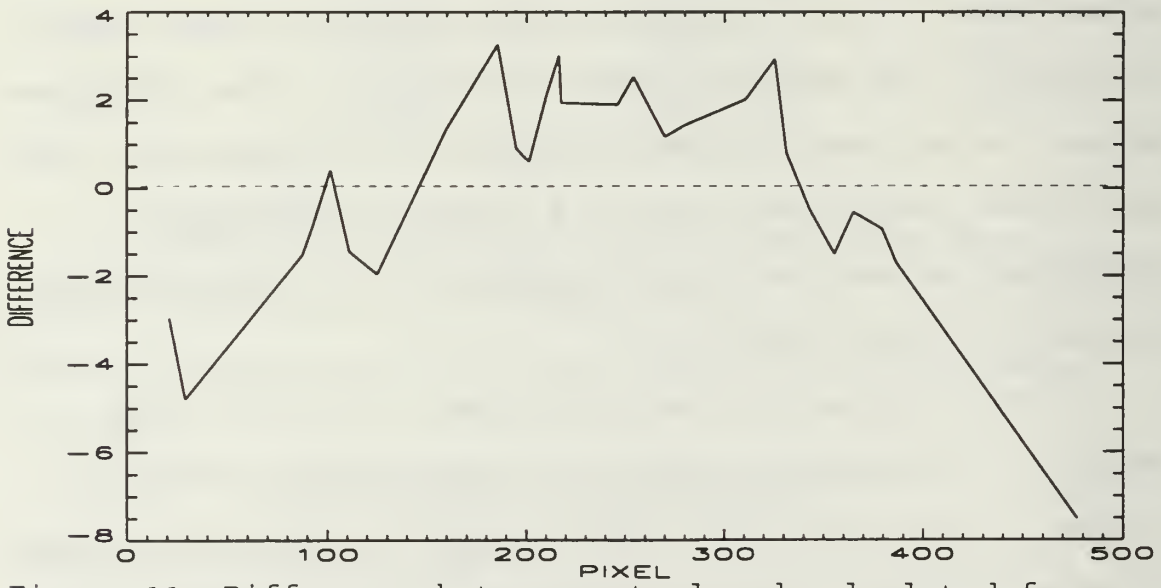

Figure 11: Difference between actual and calculated for a linear fit.

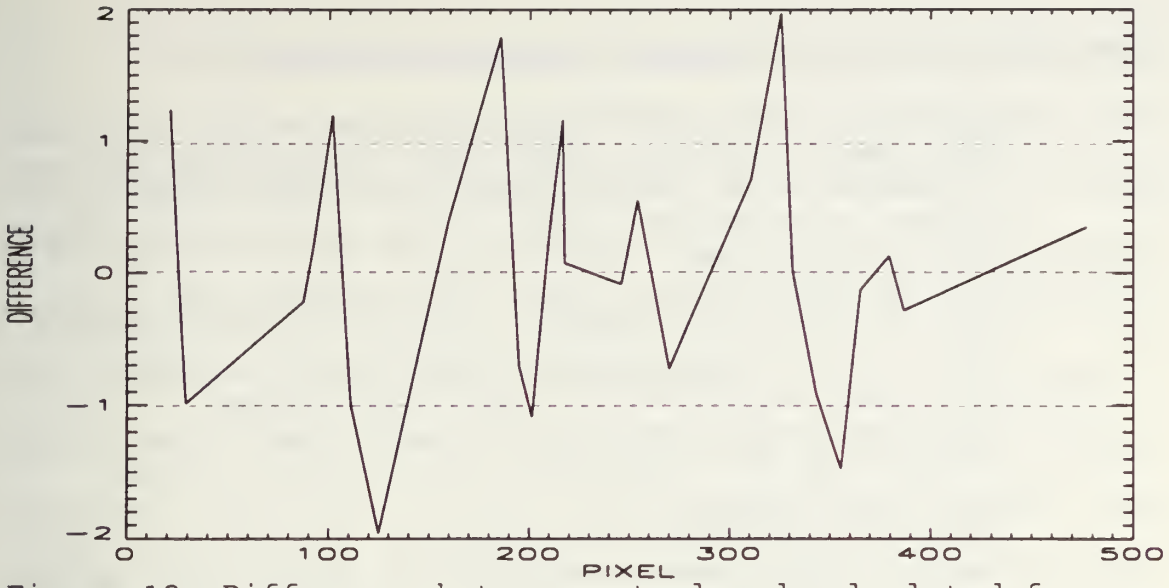

Figure 12: Difference between actual and calculated for a third degree fit.

B. DATA COLLECTION

The laboratory Ground Support Equipment (GSE) provides the same timing signals that the rocket telemetry delivers to the instrument during flight and also collects the data from the MUSTANG instrument. The GSE is controlled by a Macintosh computer equipped with National Instruments Direct Memory Access (DMA), Multi-function Input/Output (MIO) and Digital Input/Output (DIO) expansion cards. Timing signals and data acquisition are performed by 'Labview', also by National Instruments. Power is provided to the instrument in the laboratory by a Hewlett-Packard 6206 DC Power Supply.

The GSE operating procedure is detailed below:

1. Ensure the two ribbon cables are connected from the Macintosh to GSE box, one 37-pin cable from GSE box to MUSTANG, two banana cables from power supply to GSE box, and the 9-pin and 15-pin cables from the 5V and 15V converter.
2. Turn on Macintosh and find the 'MUSTANG GSE' file. Open this file and double click on the 'MAIN GSE' icon to launch Labview and the MUSTANG program.
3. Click the run button to start the program.
4. Click on the initialize I/O Boards icon. This initializes the data acquisition boards in the Macintosh computer.
5. Click on the Initialize Telemetry Clocks icon. This ensures that the data acquisition boards provide the correct telemetry signals to the MUSTANG instrument.
6. Turn on the power supply (28 Volts).
7. Turn on the amp switch and high voltage switch on the GSE box. The amp switch turns on the linear array detector and the high voltage switch turns on the image intensifier. This energizes the MUSTANG instrument.
8. Click on the Data Acquisition icon. This launches the data acquisition program. It is important that step 7 be executed before step 8. If the MUSTANG instrument is not powered it will not return a signal. The data acquisition program will wait for signals in an infinite loop.
9. Click on the Reacquire to get a new spectrum.
10. Click on the save icon. This saves the spectrum. A new spectrum can be generated by clicking on the Reacquire icon.
11. Click on the Quit icon. This stops the data acquisition subroutine and returns to the GSE panel window. Now click on the Quit icon on the main GSE Panel Window. This stops the Labview program.
12. Turn off the power supply and turn off the amp and high voltage switches on the GSE box.

C. SENSITIVITY CALIBRATION

1. Overview

The output of the instrument is 512 analogue voltages which are expressed in decimal units per pixel.

In order to convert this output in units of relative intensity to an absolute intensity (Rayleighs/Angstrom) for use in measuring the atmospheric emission rate, the raw data must be multiplied by a conversion factor. The sensitivity calibration was performed to determine this factor which is the product of the screen reflectance and the irradiance from a known light source divided by the instrument output obtained from these sources. This will be shown below. This factor is actually a function of wavelength and is the so-called 'calibration curve'.

To obtain this curve two sources of known irradiance were used. The EG&G Gamma Scientific deuterium lamp, serial number 0155, was used to cover the wavelength range of 2000 Å to 2700 Å and an Optronics Laboratories, Inc., tungston filament quartz halogen lamp (FEL-IR), serial number F-309, was used to cover from 2700 Å to 3400 Å range. The calibrations of both lamps are traceable to the National Institute of Science and Technology (NIST). Because the calibration was performed in open air, wavelengths below 2000 Å are affected by absorption due to oxygen. Therefore, no sensitivity was calculated in this region.

The first requirement was to convert the irradiance of the sources to a more useful unit. The irradiance data provided for both lamps from the manufacturer was in terms of spectral irradiance [uW/cm^2*nm] at 50 cm. Because the output of the detector is determined by the number of

photons that strike each photodiode, the output of the two calibration sources had to be converted to a photon flux. Using a spreadsheet the manufacturer's irradiance values were converted to a photon flux by dividing by the photon energy at each wavelength. This resulted in irradiance values in units of (ph/cm^2*s*Å). These irradiance values were then multiplied by the ratio (50/distance)^2 because the manufacturer data for each source were calculated at 50 cm. These points were then fit with a curve. It required two equations to fit the deuterium data at 200 cm using Poly_fit, they are:

$$E_\lambda(\lambda < 2400) = 43.395318\lambda^2 - 189935.39\lambda + 4.7551685x10^8 \qquad (4\text{-}2)$$

$$E_\lambda(\lambda \geq 2400) = -0.049545784\lambda^3 + 546.11434\lambda^2 - 2082569.0\lambda + 2.8060629x10^9 \qquad (4\text{-}3)$$

in [ph/cm^2*s*Å] at 200 cm and λ in Angstroms.

The FEL-IR source is considered a 'black-body' radiator with a temperature of approximately 3000 K. To obtain the best fit to the data we used a temperature of T=3008 K in the following eqation for a black-body radiator:

$$E_\lambda = \frac{2\pi ch}{\lambda^5} * \frac{1}{e^{hc/kT\lambda} - 1}; \qquad (4\text{-}4)$$

where c=3x10^8(m/s), h=6.626x10^{-34}(joule*sec), k=1.381x10^{-23} (joule/k). This equation yields irradiance values in

[uW/cm^2*nm] using λ in meters. Then, converting this to (ph/cm^2*s*Å) at 300 cm:

$$E_\lambda = \frac{2\pi ch}{\lambda^5}\frac{1}{e^{hc/kT\lambda}-1}\frac{10^{-7}*0.028*\lambda}{hc} \qquad (4\text{-}5)$$

yields the equation used to fit the FEL-IR irradiance data at 300 cm. These curves are shown in Figures 13 and 14 for the D2 and FEL-IR lamps, respectively.

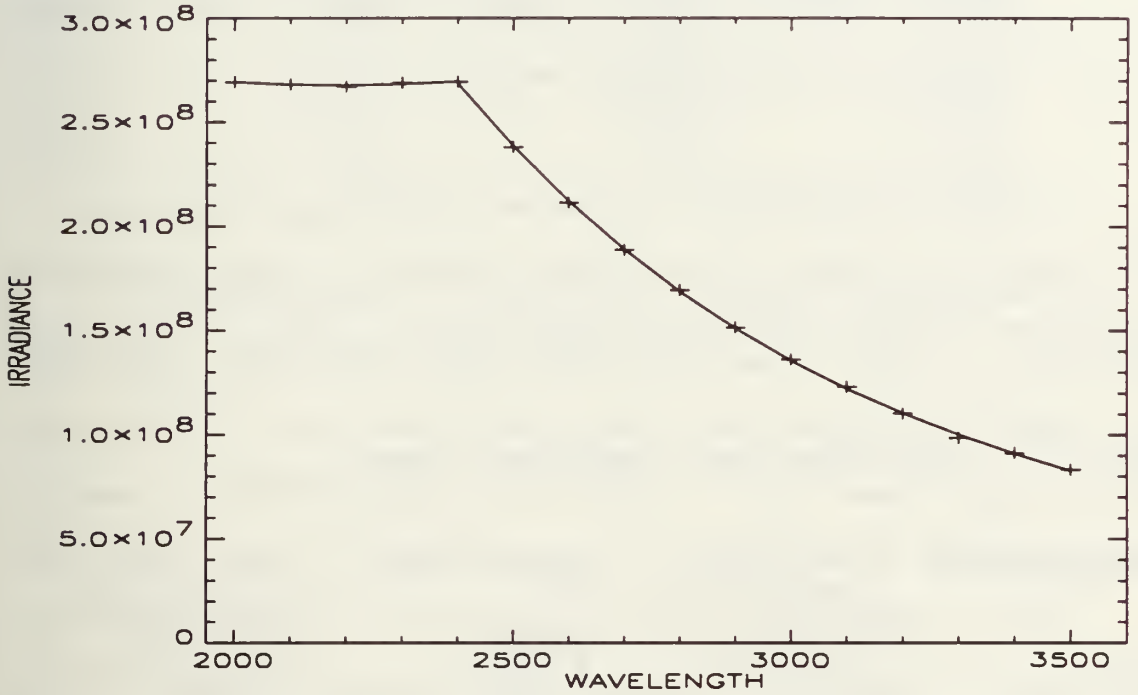

Figure 13: Curves fit to Deuterium lamp data at 200 cm.

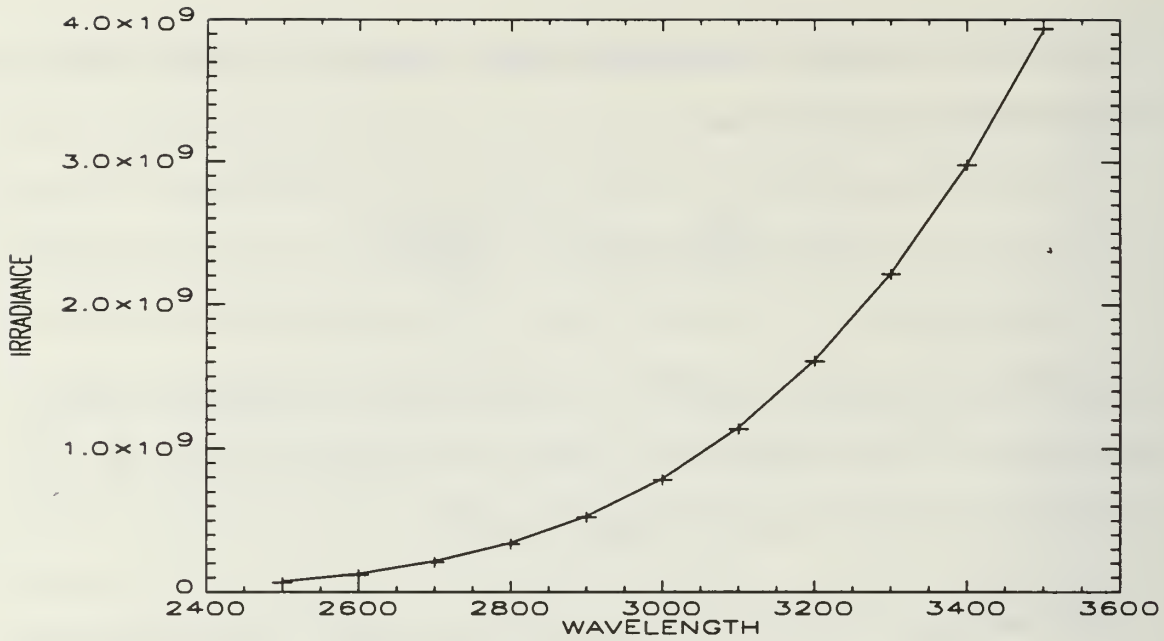

Figure 14: Curve fit to FEL_IR data at 300 cm.

These calculations produced irradiance values for the sources in units of (photons/ $cm^2*s*Å$) at the respective distances. These values are tabulated in Tables II and III.

TABLE II. IRRADIANCE FROM DEUTERIUM SOURCE

Wavelength(Å)	Irradiance (uW/cm^2*nm) at 50 cm	Energy($x10^{-19}$) (J/ph)	Irradiance ($ph/cm^2*s*Å$) at 200 cm
2000	$4.246x10^{-2}$	9.9320	$2.6933x10^8$
2100	4.027	9.4620	2.6813
2200	3.83	9.0310	2.6718
2300	3.69	8.6430	2.6897
2400	3.542	8.2825	2.694
2500	3.006	7.9512	2.3818
2600	2.566	7.6400	2.1159
2700	2.02	7.3550	1.8861
2800	1.908	7.0960	1.694
2900	1.647	6.8510	1.5145
3000	1.431	6.6210	1.3616
3100	1.253	6.4080	1.2319
3200	1.087	6.2080	1.1031

3300	9.426×10^{-3}	6.0200	9.8644×10^{7}
3400	8.457	5.8430	9.1184
3500	7.499	5.6760	8.3234

TABLE III. IRRAIDANCE FROM FEL-IR SOURCE

Wavelength(Å)	Irradiance (uW/cm^2*nm) at 50 cm	Energy($\times 10^{-19}$) (J/ph)	Irradiance ($ph/cm^2*s*Å$) at 300 cm
2500	1.87×10^{-2}	7.9512	6.5853×10^{7}
2600	3.26	7.6400	1.1947×10^{8}
2700	5.41	7.3550	2.0595
2800	8.49	7.0960	3.35
2900	1.28×10^{-1}	6.8510	5.2313
3000	1.85	6.6210	7.8235
3100	2.60	6.4080	1.136×10^{9}
3200	3.56	6.2080	1.6056
3300	4.76	6.0200	2.2139
3400	6.22	5.8430	2.9806
3500	7.98	5.6760	3.9365

For MUSTANG to record the intensity spectrum for each lamp, the lamps were placed one at a time in a closed box with an adjustable aperature. The lamp, reflecting screen and MUSTANG were all raised to the same height as the aperture. The instrument line-of-sight was 45 degrees from the normal to the reflecting screen. The normal to the screen was in line with the lamp optical axis. The lab was then darkened, the reflecting screen was fully illuminated by adjusting the box aperature and the spectra were taken using the GSE. This geometry is shown in Figure 15. The instrument output for each lamp is shown in Figures 16 and 17 for D2 and FEL_IR, respectively.

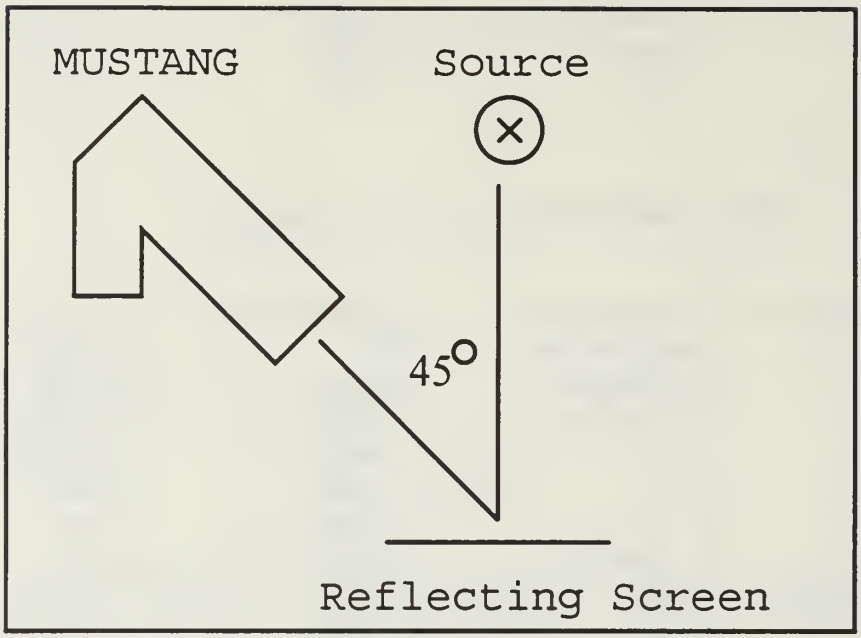

Figure 15: Geometry for collecting lamp spectra.

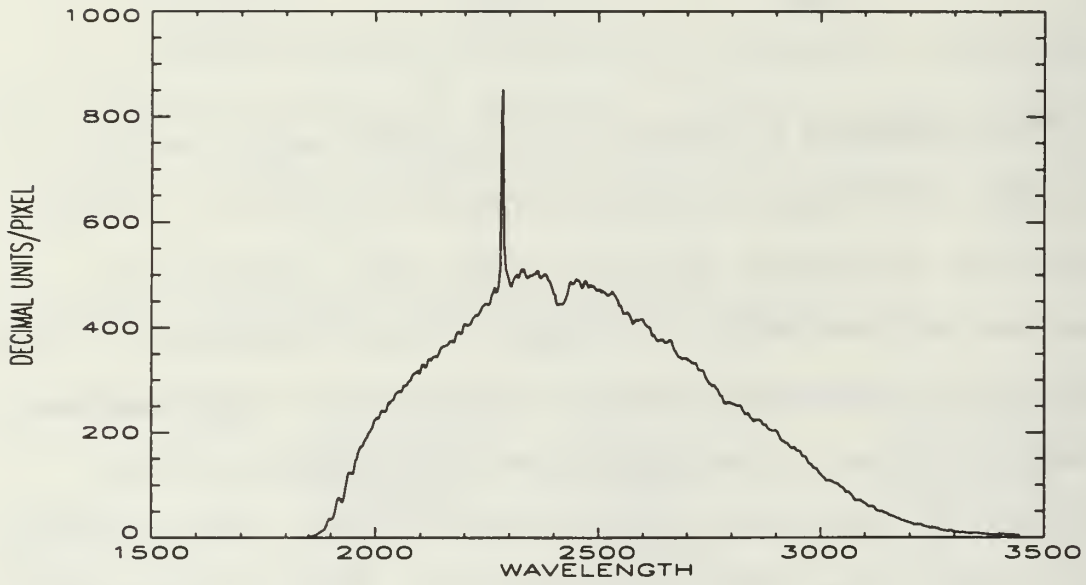

Figure 16: MUSTANG output for Deuterium lamp.

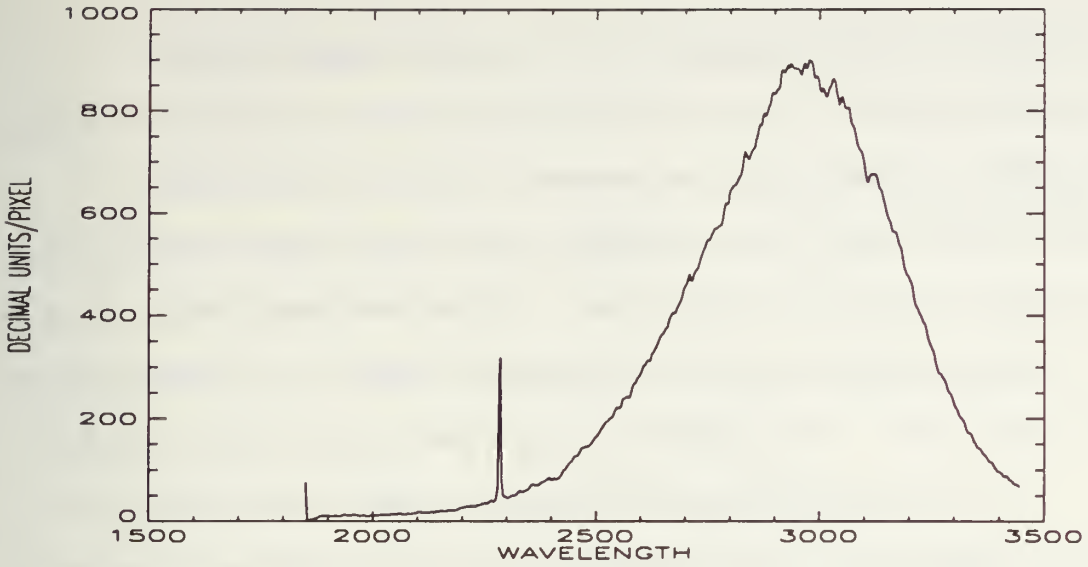

Figure 17: MUSTANG output for FEL-IR lamp.

2. Calibration Geometry and Theory

Several characteristics of the calibration were established previously (Anderson,1990; Chase,1992) and will be assumed in this calibration. First, it is assumed that the response of the MUSTANG instrument changes linearly with changes in irradiance. This linearity of response is accurate up to approximately 940 decimal units/pixel (Chase,1992). Second, it is assumed that with a viewing angle of 45°, the reflecting screen is Lambertian and no correction to the data is necessary. Finally, the field of view (FOV) of the instrument was established as 0.06° horizontal FOV, and 2.0° vertical FOV.

The output of the MUSTANG instrument is proportional to the number of photons entering the instrument. If the output and the number of photons entering is known, the

constant of proportionality, Ψ, can be determined. Tabulated above is the number of photons leaving the source. Now what is needed is the number of photons from the reflecting screen entering the instrument. This is done by dividing the reflecting screen into elemental units of area and then integrating over the area viewed by the instrument. Following this, the objective is to determine this photon flux in terms of instrument constants and the tabulated source irradiance. The instrument output is then equated to this photon flux and solved for in terms of the source irradiance, screen reflectivity and the proportionality constant. Since the instrument output is known, the constant can then be solved for.

The calibration parameter, Ψ, was defined and derived previously (Anderson, 1990; Chase, 1992). The following definitions will be used in this discussion:

E_λ -spectral irradiance $\left(\frac{ph}{cm^2 * s * \mathrm{A}}\right)$ striking the screen;

L_λ -spectral irradiance $\left(\frac{ph}{cm^2 * s * \mathrm{A} * str}\right)$ leaving the screen;

P_λ -photon flux $\left(\frac{ph}{s * \mathrm{A}}\right)$ received at the entrance slit over a one-Å wide wavelength bin;

A_t -area (cm^2) of the telescope aperature;

A_s -area (cm^2) of the spectrograph entrance slit;

A_v -area (cm^2) of the screen viewed by the instrument;

β -focal length (cm) of the telescope collecting mirror;

d -distance (cm) from the Ebert mirror to the screen;

ρ_λ -reflectance of the screen;

I -atmospheric emission rate (R/Å);

Γ -instrument gain (decimal units/photon*second);

B_W -bandwidth of each pixel (Å/pixel);

D -instrument output (decimal units/pixel).

For simplicity the λ-subscripts will be deleted; spectral irradiance/radiance and the photon flux will be implied unless otherwise stated.

The geometry of the calibration setup is shown above in Figure 15. Geometric optics allows for the calculation of the area of the screen viewed by the instrument, A_V, in the limit where the slit is narrow and $d \gg \beta$. This allows the use of plane wave assumptions. It can be shown that the solid angle viewed by the telescope (i.e. the instrument field-of view) is: $\Omega = (A_s / \beta^2)$. Similarly, the area of the screen viewed by the slit is given by: $\Omega = (A_v \cos\theta / d^2)$. Equating these two solid angles and solving for A_V gives:

$$A_v = A_s \left(\frac{d^2}{\beta^2} \right) \left(\frac{1}{\cos\theta} \right). \qquad (4\text{-}6)$$

This yields the area of the screen viewed by the instrument. Next, the irradiance leaving the reflecting screen is

needed. For a Lambertian surface, an ideal diffuse reflector, the radiance at an angle θ from the normal of the screen is equal to the product of the irradiance at $\theta = 0^o$ times the cosine of θ :

$$L(\theta) = L_o \cos\theta \ . \qquad (4\text{-}7)$$

The area of the screen viewed by the instrument must be divided into elemental units of area (da). The solid angle subtended by the telescope aperture at each element of area (da) on the screen is: $\omega = (A_t / d^2)$. The number of photons per second per angstrom received at the telescope mirror due to an element of area is: $dP = L(\theta)\omega da$. Substituting for ω yields: $dP = L(\theta)(A_t / d^2)da$. The total number of photons received at the entrance slit of the spectrograph from the reflecting screen may be calculated by integrating over the area of the screen that is viewed by the instrument. This is just the projected area of the slit on the screen. Ignoring reflective losses from the mirror, and assuming that $L(\theta)$ is constant over the elemental area in question:

$$P = L(\theta)\frac{A_t}{d^2}\int da \ . \qquad (4\text{-}8)$$

The integral is equal to A_V.

Hence:

$$P = L(\theta)\frac{A_t}{d^2}A_v . \qquad (4\text{-}9)$$

Substituting Equation (4-6) into (4-9) yields:

$$P = L(\theta)\frac{A_t}{d^2}\left(\frac{d^2}{\beta^2 * \cos\theta}\right)A_s . \qquad (4\text{-}10)$$

Rearranging the terms and simplifying leaves:

$$P = \left(\frac{A_t A_s}{\beta^2}\right)\left(\frac{L(\theta)}{\cos\theta}\right). \qquad (4\text{-}11)$$

For a Lambertian surface, where $L(\theta) = L_o \cos\theta$:

$$P = L_o\left(\frac{A_t A_s}{\beta^2}\right). \qquad (4\text{-}12)$$

Thus, the number of photons per second per Angstrom passing through the entrance slit of the spectrograph is a product of constants (for constant radiance) and is independent of angle. For this reason, the angle of the line of sight of the instrument from the normal to the reflecting screen is not important.

The spectral radiance of the screen is determined by equating the spectral irradiance striking the screen to the

total spectral radiance leaving the screen divided by the reflectivity of the screen:

$$E = \frac{\int L(\theta)\, d\Omega}{\rho}; \qquad (4\text{-}13)$$

where $d\Omega = \sin\theta d\theta d\phi$, θ ranges from 0 to $\pi/2$, and ϕ ranges from 0 to 2π. This forms a hemisphere centered on the center of the reflecting screen. Assuming that the reflectance is independent of θ, Equation (4-13) becomes:

$$E = \frac{1}{\rho} \int_0^{2\pi} \int_0^{\pi/2} (L_o \cos\theta) \sin\theta d\theta d\phi \ . \qquad (4\text{-}14)$$

The solution of this integral is: $E=\pi L_O/\rho$. Therefore, the radiance reflected normal to the screen is:

$$L_o = \frac{\rho E}{\pi} . \qquad (4\text{-}15)$$

The directional spectral radiance can now be rewritten as:

$$L(\theta) = \frac{\rho E}{\pi} \cos\theta \ . \qquad (4\text{-}16)$$

Substituting Equation (4-15) into Equation (4-12) gives:

$$P = \left(\frac{A_t A_s}{\pi \beta^2} \right) \rho E \ . \qquad (4\text{-}17)$$

This is the photon flux per Angstrom passing through the entrance slit.

Converting the raw data (decimal units/pixel) to a standard unit (R/Å) is done by equating the flux entering the spectrograph, P, to the instrument output, D as follows:

$$D=P\Gamma B_W; \tag{4-18}$$

where Γ is the instrument gain, a product of the various efficiencies and transfer functions of the individual components of the instrument, and B_W is the bandwidth of each pixel. See the Appendix for a definition and derivation of Γ. Substituting for the flux, Equation (4-17), yields:

$$D = \Gamma B_w \left(\frac{A_l A_s}{\pi \beta^2} \right) \rho E . \tag{4-19}$$

The constants in Equation (4-19) are gathered together to define a new constant:

$$K = \Gamma B_w \left(\frac{A_l A_s}{\pi \beta^2} \right) \rho ; \tag{4-20}$$

which allows the output of the instrument to be written in terms of the source irradiance and constants:

$$D=KE. \tag{4-21}$$

Now, assuming that the atmospheric emission rate is omnidirectional or $4\pi I$ (R/Å), the spectral radiance received by the MUSTANG instrument is:

$$L = \left(\frac{10^6 I}{4\pi} \right); \tag{4-22}$$

where L is in units of $\left(\frac{ph}{cm^2 sAstr} \right)$. The spectral radiance recieved by MUSTANG may also be written in terms of the spectral irradiance of the atmosphere. For normal incidence this is:

$$L = E/\pi. \tag{4-23}$$

With omnidirectional emissions the instrument is at normal incidence to the atmospheric airglow regardless of the OZA. This removes any angular dependence from the calculations. Therefore, the output of the instrument, Equation (4-19), due to the spectral radiance received from the atmosphere is:

$$D = \Gamma B_w \left(\frac{A_t A_s}{\beta^2} \right) L. \tag{4-24}$$

This is rewritten in terms of the omnidirectional emission rate, Equation (4-22):

$$D = \Gamma B_w \left(\frac{A_t A_s}{\beta^2} \right) \left(\frac{10^6 I}{4\pi} \right). \qquad (4\text{-}25)$$

Solving for the emission rate of the atmosphere yields:

$$I = \left(\frac{1}{10^6} \right) \left(\frac{4\pi\beta^2}{B_w \Gamma A_t A_s} \right) D; \qquad (4\text{-}26)$$

where I is in units of R/Å. This atmospheric emission rate is now in terms of instrument constants and the output. So, given the output of the instrument, the atmospheric emission rate can now be determined.

A new constant is defined:

$$\Psi = \left(\frac{4\pi\beta^2}{10^6 B_w \Gamma A_t A_s} \right). \qquad (4\text{-}27)$$

This is simplified by using the definition for K from Equation (4-20), which yields:

$$\Psi = \left(\frac{4\rho}{10^6 K} \right). \qquad (4\text{-}28)$$

Substituting this constant into Equation (4-25), where E is the spectral irradiance from a calibration source, yields:

$$D=\left(\frac{4\rho}{10^6}\right)\left(\frac{E}{\Psi}\right). \qquad (4\text{-}29)$$

The instrument output is now defined in terms of the source irradiance, the reflectivity of the screen and the proportionality constant. The constant, Ψ, may then be defined in terms of the screen reflectance, spectral irradiance and the response of the instrument as:

$$\Psi=\left(\frac{4\rho}{10^6}\right)\left(\frac{E}{D}\right); \qquad (4\text{-}30)$$

in units of (Rayleighs/Angstrom)/(decimal units/pixel). This results in the calibration parameter, Ψ, for the MUSTANG instrument.

Finally, the spectral emission rate, which will be used below, for the atmosphere is equal to the calibration parameter multiplied by the detector response:

$$I=D\Psi. \qquad (4\text{-}31)$$

This constant, Ψ, is dependent on wavelength and is the calibration curve needed to convert from decimal units/pixel to Rayleighs/Angstrom. With the irradiance values calculated above and the instrument output already obtained, the only

necessary input remaining is the reflectance, ρ, of the screen.

3. Reflectivity of screen as a function of wavelength

The first step in calculating the screen reflectance curve is to take the ratio of the instrument output from the reflecting screen to the instrument output looking directly at the lamp. This was done for each lamp individually. Because of the sensitivity of the instrument, looking directly at each lamp would completely saturate the output. To obtain useable output, the instrument entrance was covered with a piece of cardboard with a tiny pinhole aperature. This reduced the incoming photon flux to useable levels.

Next, the relative reflectance curve for each lamp was normalized. This was accomplished using information from the manufacturer concerning the reflectance of the Barium Sulfate surface coating of the screen. At wavelengths longward of 3200 Å, this reflectance is considered constant at 0.97. The FEL-IR ratio curve was then normalized to 0.97 by multiplying by 0.366. The Deuterium ratio was then multiplied by 0.70764 to acheive the same normalization. These two individual curves were then overlapped to arrive at the reflectance curve. The useable portion of the deuterium curve was from pixel 47 to 350 (2000 Å to 2951 Å). The usable portion of the FEL-IR curve was from pixel 250 to

450 (2640 Å to 3259 Å), this yielded an overlap of 311 Å. Outside of these ranges the normalized curves were far too noisy. This left the ranges of 1850 to 2000 Å and 3259 to 3400 Å unaccounted for. For the 3259 to 3400 Å range, the reflectance was assumed constant at 0.97. For the 1850 to 2000 Å range a line was fit to the deuterium lamp data with the equation:

$$y = .001983x + 0.34 \qquad (4\text{-}32)$$

where x is the pixel number. This final reflectance curve is shown in Figure 18.

With the reflectance curve now determined, the calibration parameter, Ψ, could now be calculated using:

$$\Psi = \left(\frac{4\rho}{10^6}\right)\left(\frac{E}{D}\right). \qquad (4\text{-}33)$$

This calibration curve was calculated individually for each lamp as shown in Figures 19 and 20. The two curves were then overlayed and merged at pixel 206, 2499.73 Å, to yield the final calibration curve as shown in Figure 21.

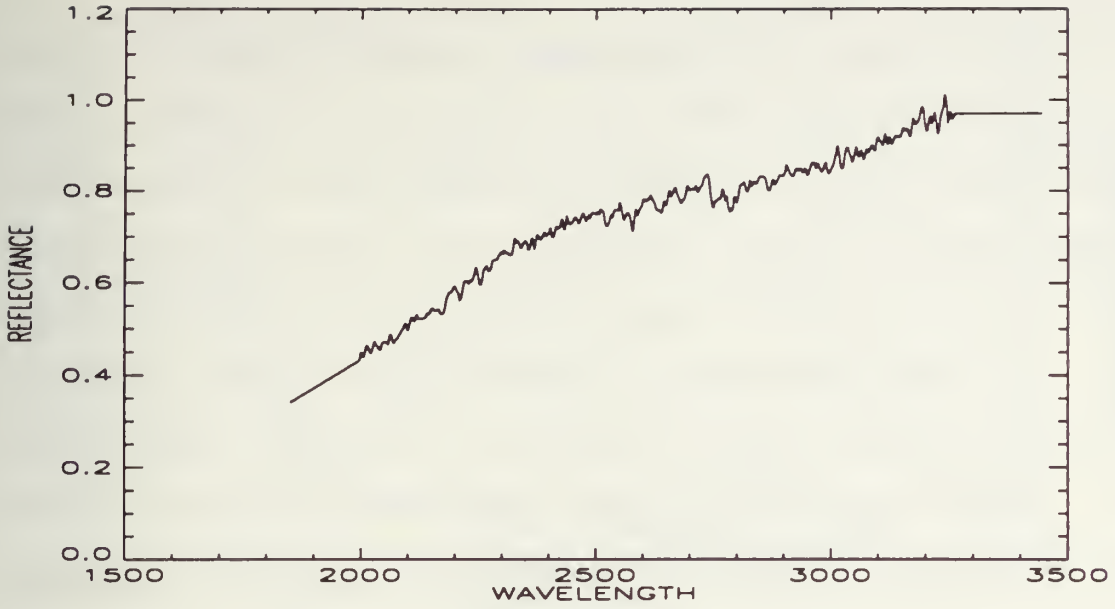

Figure 18: Reflectance curve.

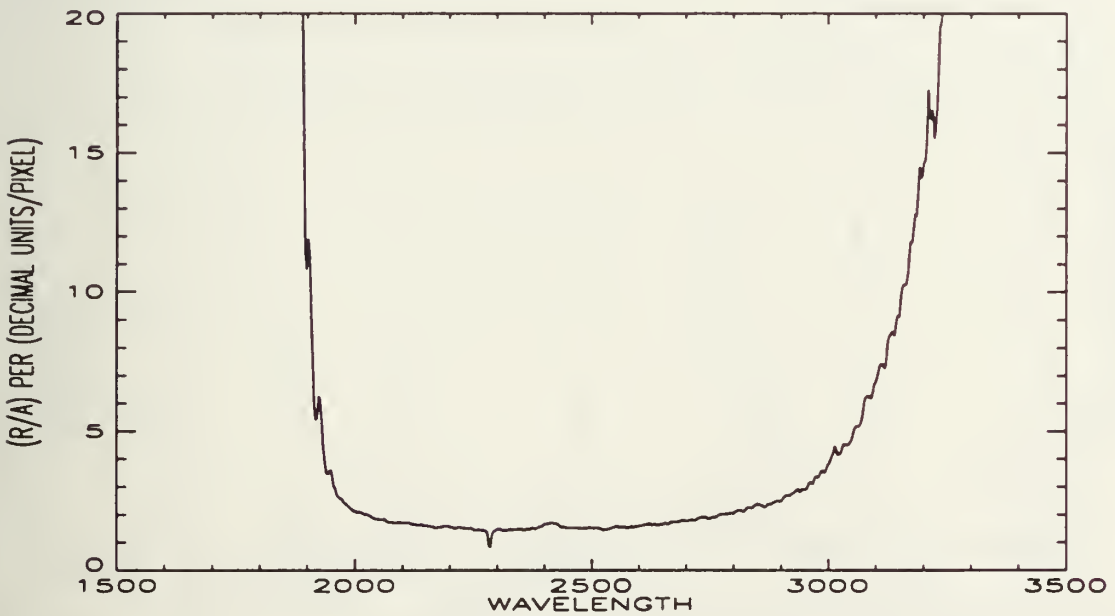

Figure 19:Deuterium lamp sensitivity curve.

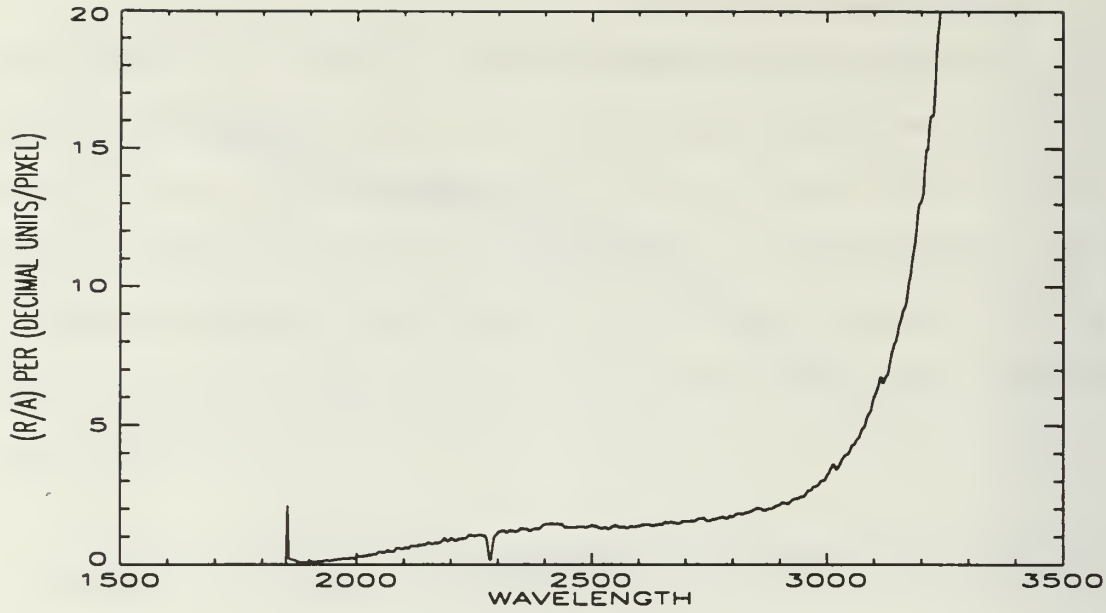

Figure 20: FER-IR sensitivity curve.

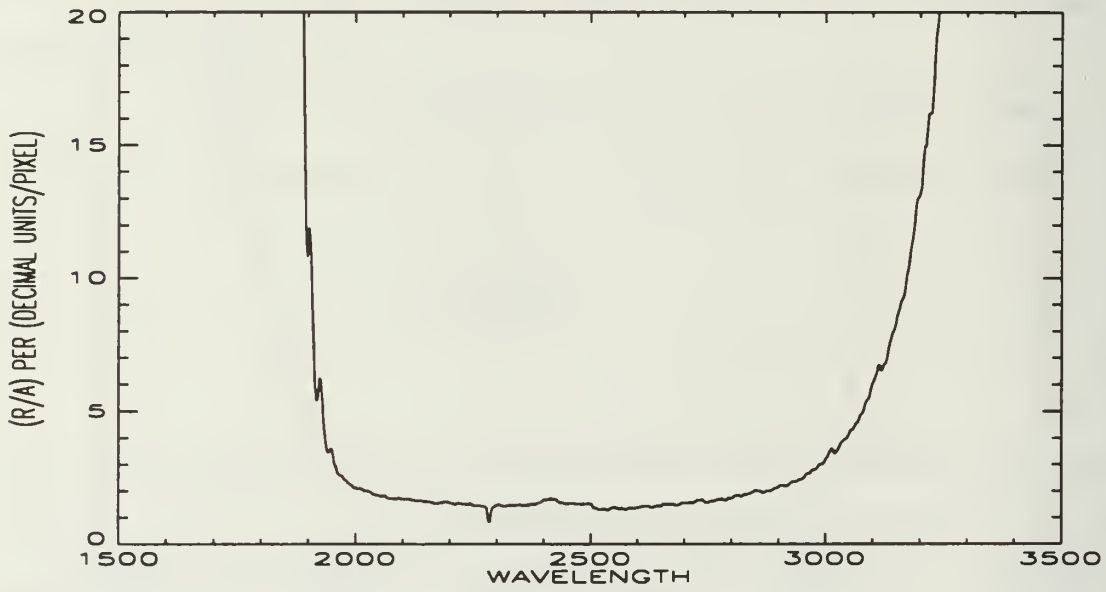

Figure 21: Final calibration parameter.

D. POST-FLIGHT CALIBRATION

Post-flight calibration indicated that the wavelength calibration did not change and there was no significant change in the sensitivity calibration as a result of the

launch. Figure 22 shows a comparison of the pre-flight and post-flight platinum spectra. For wavelength calibration, the position of each peak with respect to pixel position is the important factor, not intensity. As can be seen, the pixel position of each emission peak is essentially unchanged, indicating no change in the wavelength calibration. Figure 23 is the post-flight deuterium spectrum compared with the pre-flight deuterium spectrum. Again, the pre-flight spectrum is plotted directly over the top of the post-flight spectrum indicating no change in the sensitivity calibration.

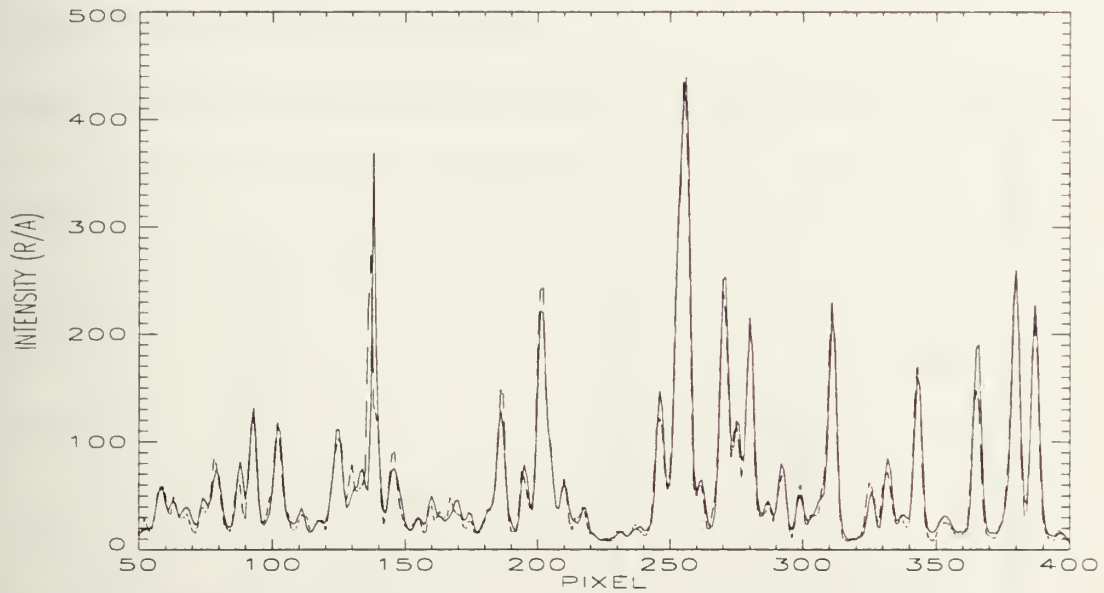

Figure 22: Post-flight platinum spectrum plotted over the pre-flight platinum spectrum.

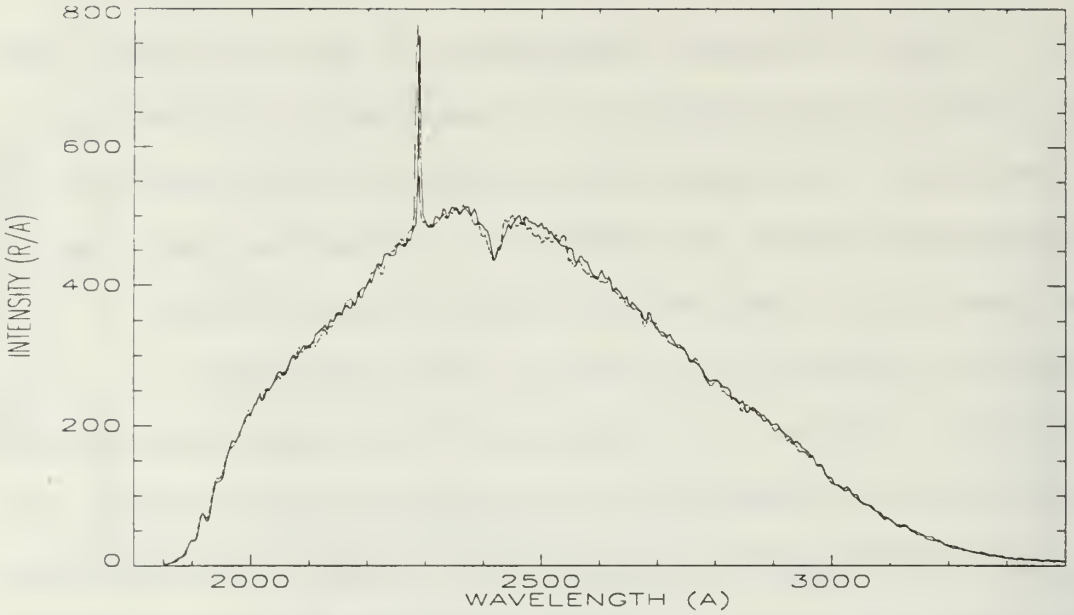

Figure 23: Pre-flight deuterium spectrum plotted over the post-flight deuterium spectrum.

V. DATA ANALYSIS

A. INTRODUCTION

The objective of this analysis is to estimate the temperature profile from the NO γ(0,1) and Vegard-Kaplan (0,5) bands, and the intensity profile for the singly ionized oxygen (OII) 2470 Å multiplet on the downleg of the March 1992 rocket experiment. The spectra for the downleg were taken from 320 km down to 115 km. Shown in Figure 24 is a representative spectrum taken at 180 km. It is a plot of intensity versus wavelength.

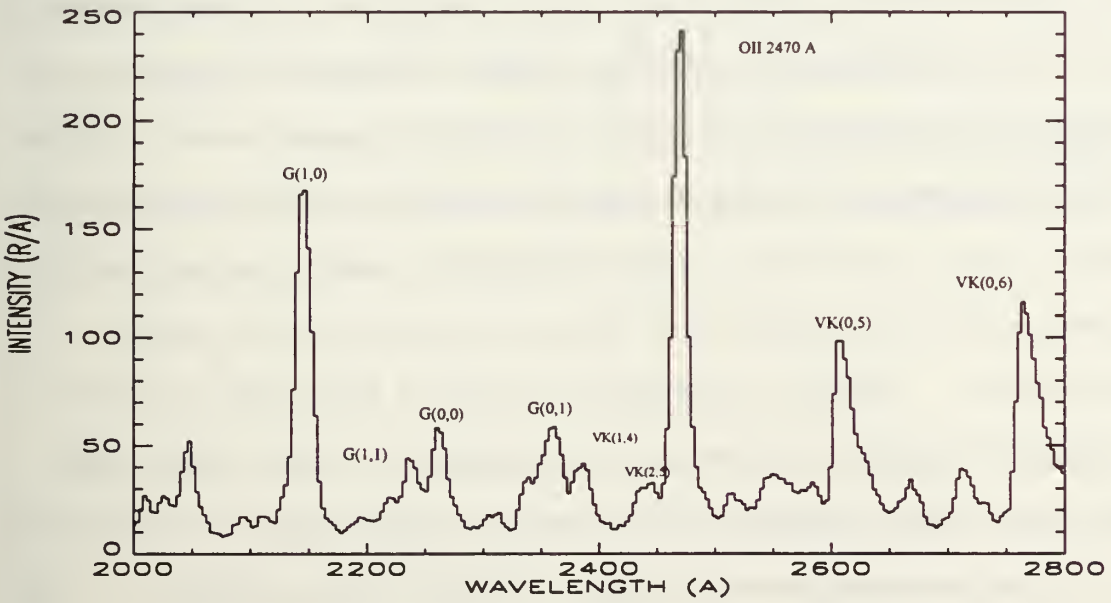

Figure 24: Representative spectrum taken at 180 km.

The determination of the 2470 Å intensity profile is complicated by the presence of contaminating emissions from the nitric-oxide gamma (γ) transition and the nitrogen (N_2) Vegard-Kaplan (VK) transition. The nitric oxide γ bands are the result of the electronic transition from the first excited state to the ground state ($A^2\Sigma^+ \rightarrow X^2\Pi$) and extend from 1873 Å to 6126 Å. As stated above, within this one electronic transition are many possible vibrational transitions. For example, $\gamma(0,6)$ refers to the transition from the zero vibrational level of the first excited state to the sixth vibrational level of the ground state. The NO γ bands are produced primarily by photo-excitation.

The molecular nitrogen (N_2) Vegard-Kaplan bands are also the result of the transition from the first excited state to the ground state ($A^3\Sigma^+_u \rightarrow X^1\Sigma_g^+$). The emissions in this transition range from 1250 Å to 5325 Å. There is a difference between this transition and the NO γ transition above. This transition is a forbidden transition and is produced by collisions with photo-electrons vice photo-excitation.

The OII 2470 Å emission is produced by the transition from the second excited state to the ground state ($^2P \rightarrow ^4S$) of singly ionized atomic oxygen. Unlike the molecular transitions described above, the 2470 Å transition involves no vibrational or rotational energy levels and does not produce a band of emissions. Like the N2 VK transition, this

transition is also forbidden and is produced by collisions with photo-electrons vice photo-excitation.

B. GENERATION OF SYNTHETIC SPECTRA

The models generating the synthetic spectra for N_2 VK and NO γ bands below were developed by Cleary (1986). These synthetic spectra are generated based on the quantum selection rules and the probabilities governing the different transitions. The probabilities of the various vibrational transitions within each electronic state are given by the Franck-Condon factors. These synthetic spectra are then convolved with the instrument slit functions to match the output of the instrument. There are five different slit functions for the MUSTANG instrument. The slit function that produced the best fit was used in the convolution. Because the OII 2470 Å emission doesn't depend on temperature, the synthetic spectrum is generated by simply inserting a delta function at the required wavelength and convolving it with a slit function.

C. FITTING THE DATA WITH THE SYNTHETIC SPECTRA

The data used to analyze the 2470 Å multiplet consisted of 42 records in 5 km increments that ranged from 115 km to 320 km. To fit each spectrum, synthetic spectra were generated for NO γ and N_2 VK bands. These synthetic spectra were multiplied by constants to match the actual intensities recorded by MUSTANG. Once the contribution from the

contaminating emissions were estimated, they could be subtracted out. The remaining feature is attributed to the OII 2470 Å emission. This feature is fit by multiplying the convolved delta function by a constant in the same manner as above.

The spectrum at each altitude was fit individually. The synthetic models require an estimated rotational temperature for the specified altitude and the vibrational transition of interest for input. By running the models repeatedly using different vibrational transitions, theoretical spectra for the NO γ and N_2 VK bands were developed. The NO γ bands contributing to the 2100 Å to 2800 Å wavelength range are: (0,0), (0,1), (0,2), (1,0), (1,1), and (1,3). The N_2 VK bands contributing to the 2100 Å to 2800 Å wavelength range are: (0,3), (0,4), (0,5), (0,6), (1,4), (2,5), and (3,6). The OII 2470 Å emission is contaminated by the VK(3,6) band and the γ(0,2) band. The synthetically generated spectra for the bands listed above are shown plotted over the 180 km spectrum in Figure 25.

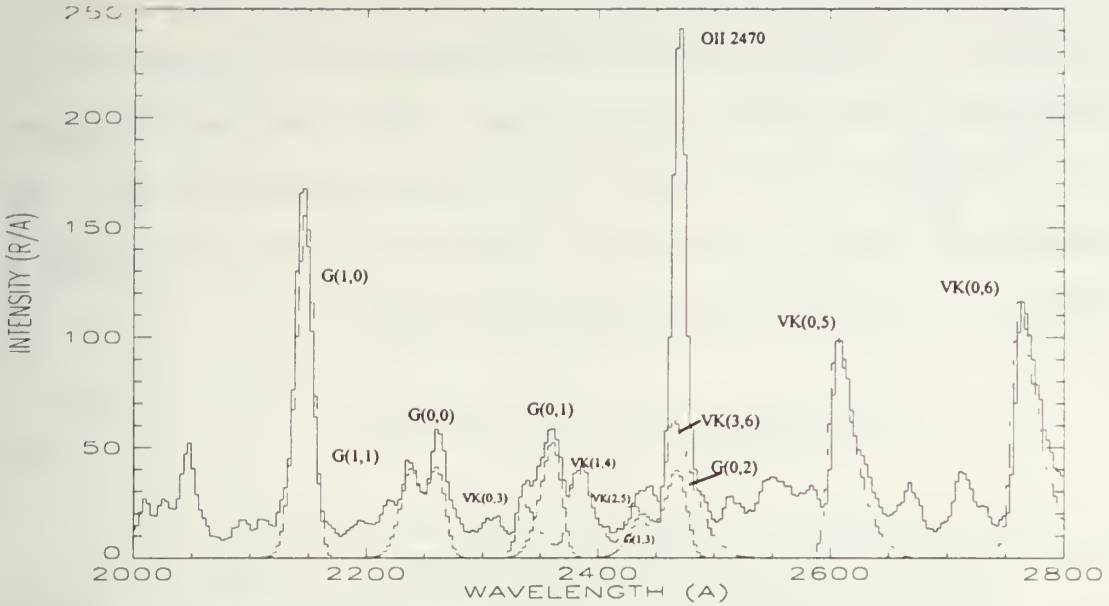

Figure 25: Synthetically generated spectra for vibrational bands of interest plotted over the 180 km spectrum.

The rotational temperature also affects the shape of the synthetic spectra. At higher rotational temperatures more molecules are in higher rotational states causing the shape of the molecular band to shift as shown in Figure 26. This temperature dependence affects NO γ and N_2 VK differently since the N_2 VK bands are degraded to the red and the NO γ bands are degraded to the blue. This means that for the synthetic N_2 VK bands, using a higher rotational temperature shifts the shape of the molecular band to longer, or 'red' wavelengths. For the synthetic NO γ bands a higher rotational temperature shifts the shape of the molecular band to shorter or 'blue' wavelengths. Since atomic oxygen emissions involve no vibrational or rotational energy states, changing the temperature has no effect on the shape of the feature. The actual atmospheric temperature at the

altitude of interest can be inferred from the rotational temperature that best fits the data. This was performed on all 42 spectra. The results are listed in Table IV and the temperature profile is shown in Figure 27. The rotational temperature profile can be modeled using:

$$T(altitude) = T_{\infty} - (T_{\infty} - T_{115}) * e^{-s(altitude-115)}, \qquad (5\text{-}1)$$

where s=0.0255/km, T_{∞}=1300 K and T_{115}=550 K. The temperature at 115 km is considerably higher than predicted by MSIS, the standard atmospheric model. More work is required to resolve this. A comparison of these two profiles is shown in Figure 28.

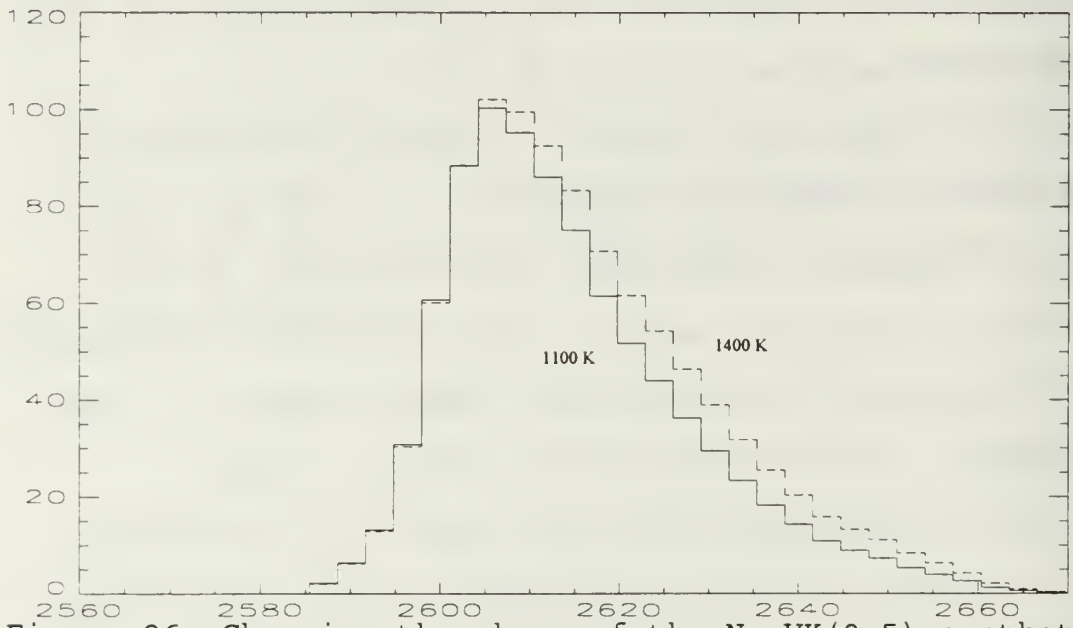

Figure 26: Changing the shape of the N_2 VK(0,5) synthetic spectrum by using a higher rotational temperature.

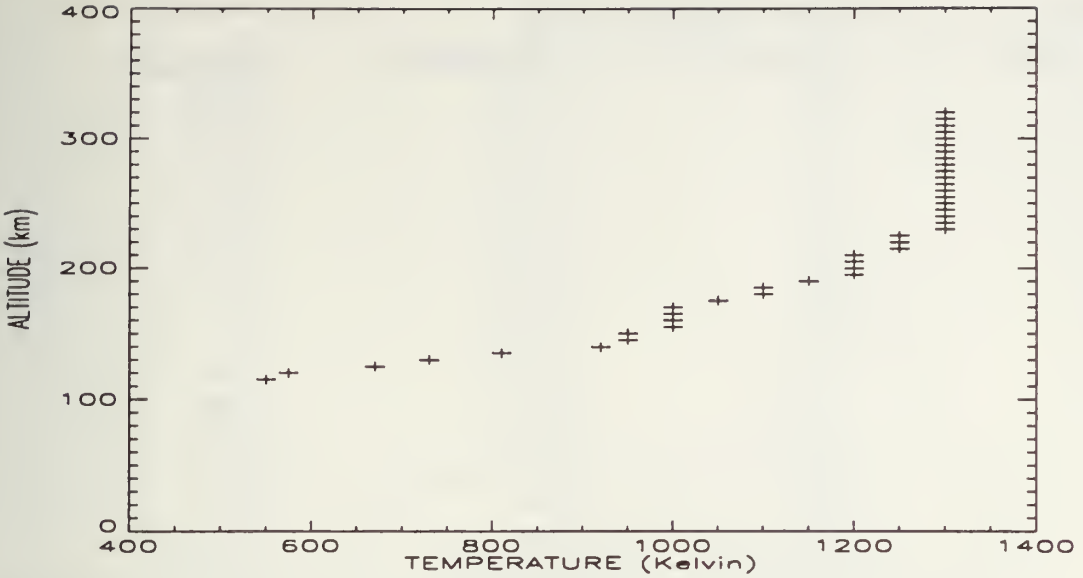

Figure 27: The estimated temperature profile for the downleg.

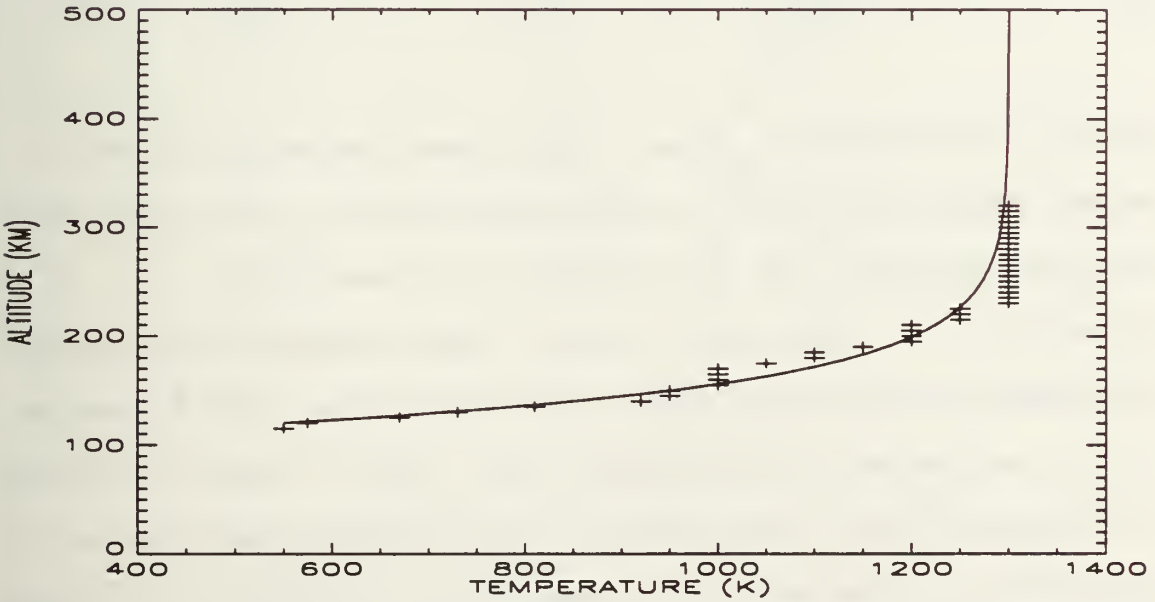

Figure 28: Comparison of temperature profile inferred from the data with profile calculated from Equation (5-1). The solid line is from Equation (5-1).

TABLE IV. ESTIMATED TEMPERATURES

Alt (km)	Temp (K)	Alt (km)	Temp (K)
115	550	220	1250
120	575	225	1250
125	670	230	1300
130	730	235	1300
135	810	240	1300
140	920	245	1300
145	950	250	1300
150	950	255	1300
155	1000	260	1300
160	1000	265	1300
165	1000	270	1300
170	1000	275	1300
175	1050	280	1300
180	1100	285	1300
185	1100	290	1300
190	1150	295	1300
195	1200	300	1300
200	1200	305	1300
205	1200	310	1300
210	1200	315	1300
215	1250	320	1300

To fit the NO and N_2 data, vibrational bands had to be chosen that showed very little contamination from other non-related emissions. By multiplying the theoretical intensities by constants to match these selected emissions the contribution from these molecules to the 2470 Å feature can be estimated and subtracted out. This is shown in Figure 29. The remaining intensity to this feature is attributed to the OII 2470 Å emission. A representative final fit is shown in Figure 30.

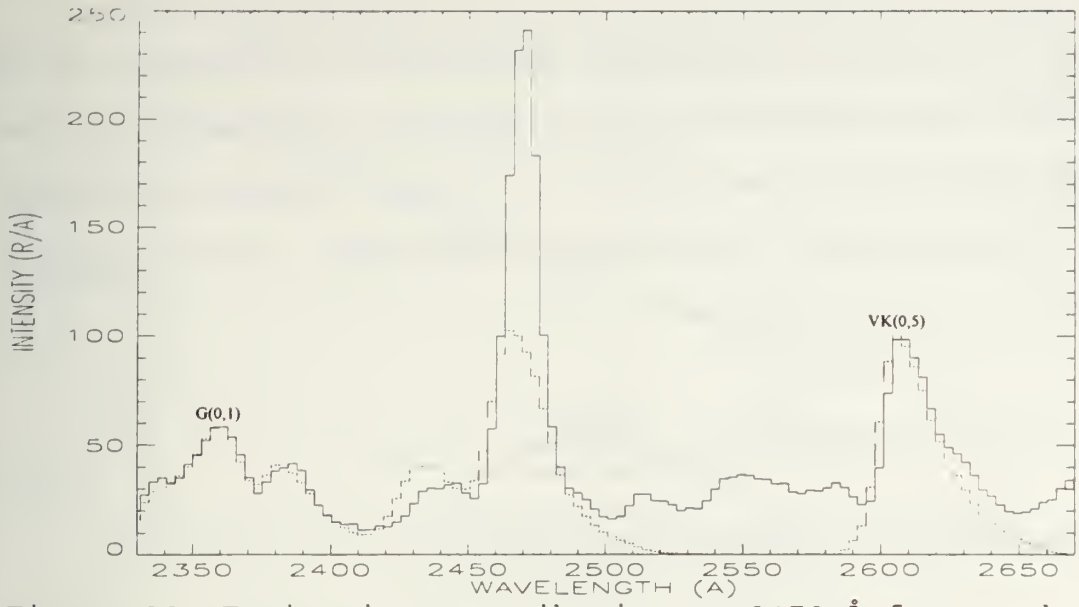

Figure 29: Estimating contribution to 2470 Å feature by NO γ and N_2 VK emissions. The solid line is the observed intensity, the dashed line is the sum of NO γ and N_2 VK.

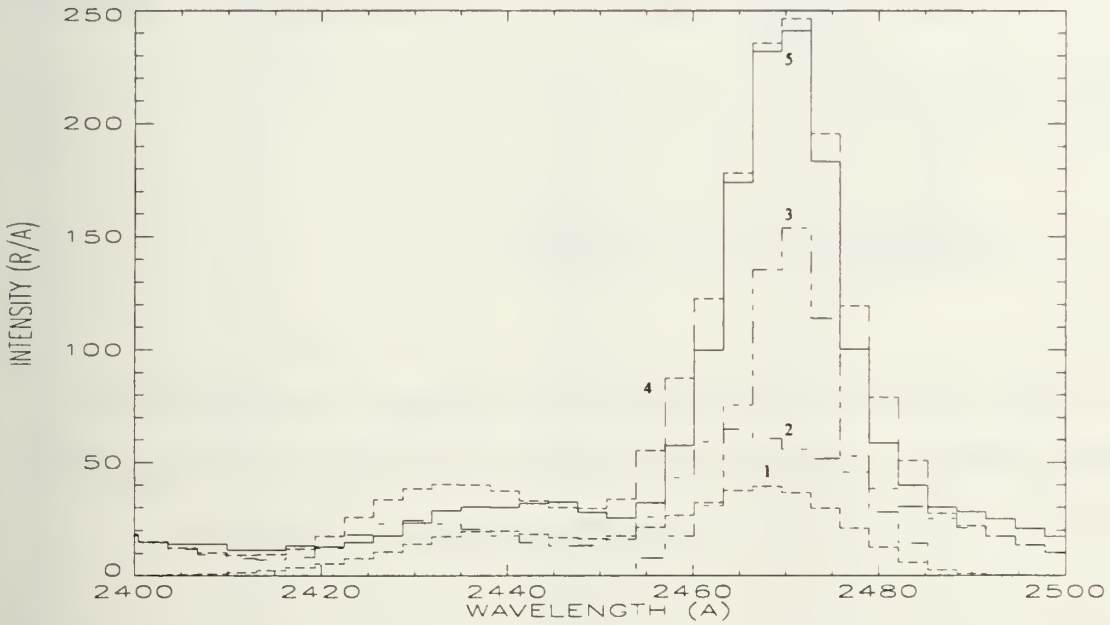

Figure 30: Representative final fit for 180 km showing contributions from all emissions. Curves presented are: 1) NO γ, 2) N_2 VK, 3) OII 2470 Å, 4) Overall fit, 5) Data.

Because the nitric oxide γ transition is an allowed transition and is produced by photo-excitation, the volume

emission rates of these bands depend on the intensity of the incoming solar radiation. This incoming solar radiation can be assumed to be constant over the rocket launch time frame. The NO scale factor can be used to estimate the NO column density by starting with:

$$Data(R/A) = Synthetic\left(\frac{photons}{pixel * molecule * \sec}\right) * Scale \quad . \qquad (5\text{-}2)$$

Solving for the scale factor yields:

$$\frac{Data}{Synthetic} = Scale\left(\frac{R/\mathrm{A}}{ph/pix * mol * \sec}\right) * \frac{10^6 \frac{ph}{cm^2 * \sec}}{1R} * 3.133\frac{\mathrm{A}}{pix} \quad ; \qquad (5\text{-}3)$$

which reduces to:

$$\frac{Data}{Synthetic} = Scale * 3.133 \times 10^6\left(\frac{mol}{cm^2}\right) . \qquad (5\text{-}4)$$

The scale factor multiplied by a constant yields the NO column density. These values for the downleg are tabulated in Table V and plotted versus altitude in Figure 31.

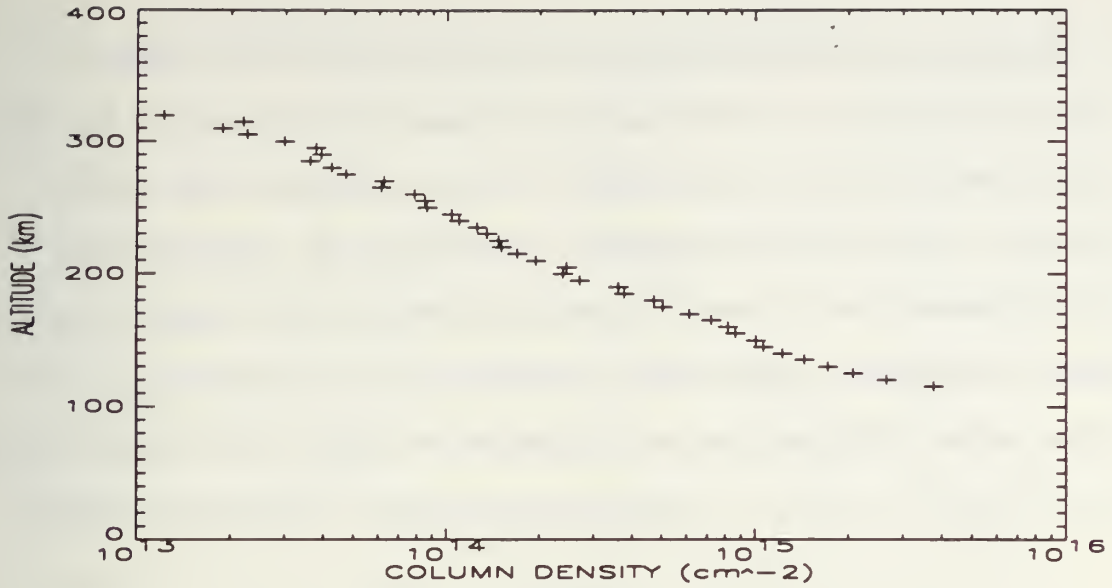

Figure 31: Estimated nitric oxide column density.

TABLE V. ESTIMATED NITRIC OXIDE COLUMN DENSITY

Alt (km)	Column Density (cm^{-2})	Alt (km)	Column Density (cm^{-2})
115	3.76e15	220	1.50
120	2.66	225	1.47
125	2.06	230	1.34
130	1.72	235	1.25
135	1.44	240	1.09
140	1.22	245	1.03
145	1.06	250	8.61e13
150	1.00	255	8.45
155	8.61e14	260	7.83
160	8.14	265	6.10
165	7.20	270	6.23
170	6.10	275	4.69
175	5.01	280	4.22
180	4.69	285	3.60
185	3.75	290	3.91
190	3.60	295	3.75
195	2.69	300	2.97
200	2.38	305	2.25
205	2.44	310	1.87
210	1.94	315	2.19
215	1.69	320	1.22

Because the N_2 VK and the OII 2470 Å are forbidden transitions, the volume emission rates are dependent on the photo-electron flux. This flux is not constant and varies greatly, so the scale factors for the N_2 VK band and the 2470 Å feature are used to estimate the intensities vice the column densities. The total intensity is solved for by integrating to find the area under the molecular band or the area under the 2470 Å feature as shown in Equation (5-5):

$$I = \int I_\lambda d\lambda \quad (5\text{-}5)$$

But, this intensity can be estimated by using the scale factor and the synthetically generated spectral emission as shown in Equation (5-6):

$$I \approx \int Syn(\lambda) * Scale * d\lambda = Scale * \Delta\lambda * \sum Syn \quad (5\text{-}6)$$

where $\Delta\lambda$=3.133(Å/pixel) and $\sum Syn$ is the total intensity or area under the synthetically generated spectral emission after it has been convolved with the slit function and before it is multiplied by the scale factor. The total intensity of the synthetically generated N_2 VK(0,5) band with a temperature of 550 K is 7.4×10^{-2}. The difference between the intensity at 550 K and 1300 K is only a few percent. As a result, this total intensity was used for all

altitudes. Because the synthetically generated spectrum for the 2470 Å feature is a delta function, the area is 1.0.

This calculation for the intensity was performed for each spectrum. The resulting intensity values for the N_2 VK(0,5) band are listed in Table VI, with the intensity profile shown in Figure 32. The resulting intensity values for the 2470 Å feature are listed in Table VII, with the intensity profile shown in Figure 33.

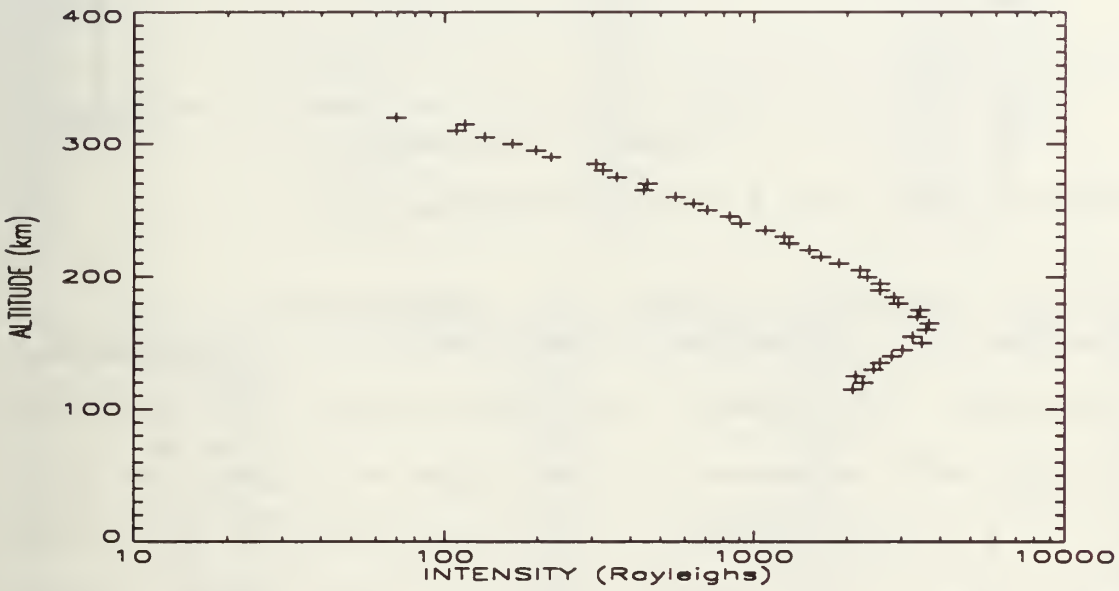

Figure 32: N_2 VK(0,5) intensity profile.

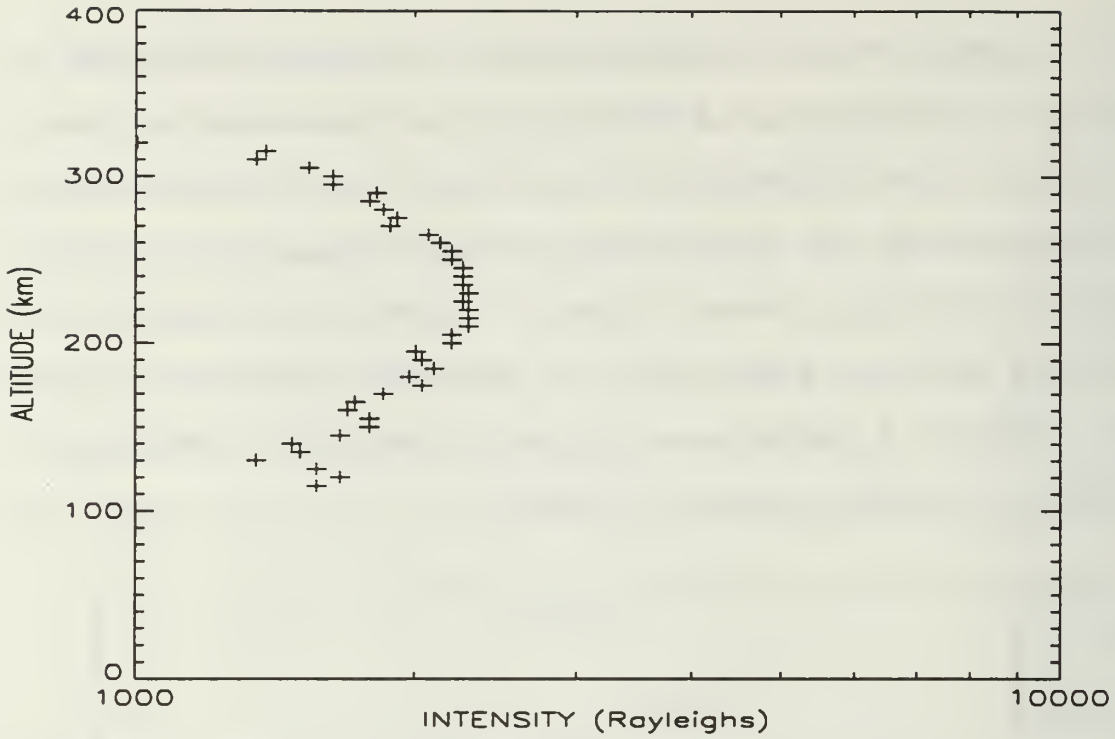

Figure 33: OII 2470 Å intensity profile.

TABLE VI. ESTIMATED NITROGEN (N_2) INTENSITIES

Alt (km)	Intensity (R)	Alt (km)	Intensity (R)
115	2090.64	220	1509.91
120	2253.24	225	1300.84
125	2137.10	230	1254.38
130	2439.08	235	1091.78
135	2555.22	240	905.94
140	2787.52	245	836.25
145	3019.81	250	708.49
150	3484.40	255	638.80
155	3252.10	260	557.50
160	3600.54	265	441.35
165	3670.23	270	452.97
170	3368.25	275	360.05
175	3437.94	280	325.21
180	2926.89	285	308.95
185	2833.98	290	220.67
190	2555.22	295	197.44
195	2555.22	300	164.92
200	2322.93	305	134.73
205	2206.78	310	109.17
210	1881.57	315	116.47
215	1649.28	320	69.68

TABLE VII. ESTIMATED OII 2470 Å INTENSITIES

Alt (km)	Intensity (R)	Alt (km)	Intensity (R)
115	1567.97	220	2289.24
120	1662.05	225	2257.84
125	1567.97	230	2289.24
130	1348.46	235	2257.88
135	1505.25	240	2257.88
140	1473.89	245	2257.88
145	1662.05	250	2195.16
150	1787.49	255	2195.16
155	1787.49	260	2132.44
160	1693.41	265	2069.72
165	1724.77	270	1881.57
170	1850.21	275	1912.93
175	2038.36	280	1850.21
180	1975.65	285	1787.49
185	2101.08	290	1818.85
190	2038.36	295	1630.69
195	2007.00	300	1630.69
200	2195.16	305	1536.61
205	2195.16	310	1348.46
210	2289.24	315	1379.82
215	2289.24	320	1003.50

In order to verify the above results, the intensity of the N_2 VK(0,5) band was estimated directly from the data using an integration approximation technique. The shape of the VK(0,5) molecular band can be approximated by a triangle. Using area=(1/2)*base*height, the intensity can be estimated. This is shown schematically in Figure 34. Using this method, the area under the N_2 VK(0,5) band at 180 km was estimated to be 2400 (R). Whereas, using the fitting method above the intensity was estimated to be 2600 (R), the difference between these values being only 7%.

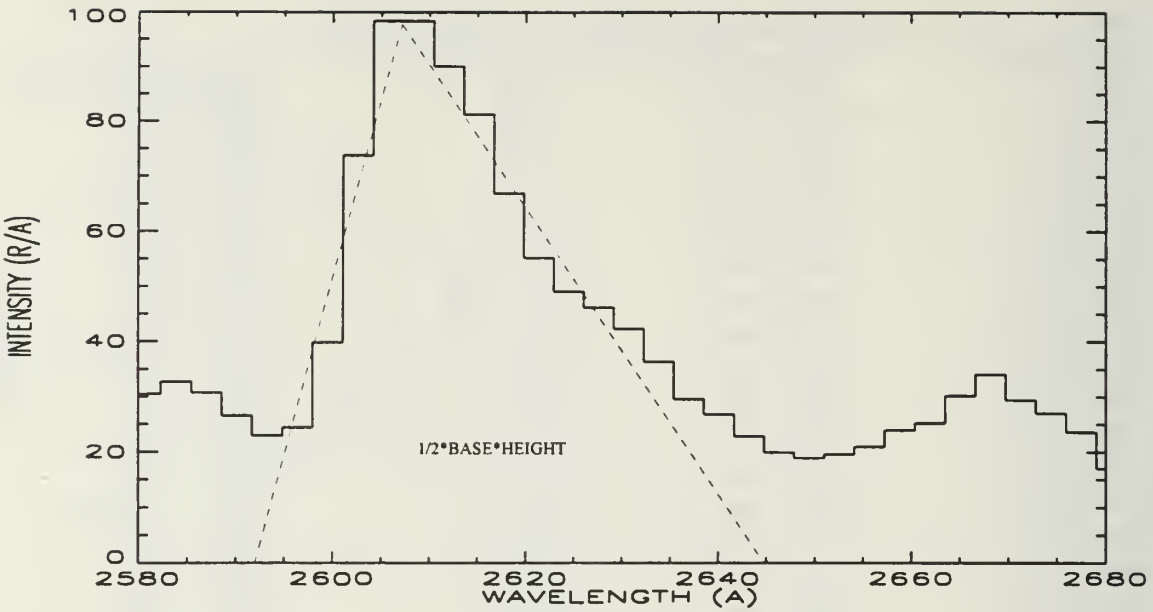

Figure 34: Use of estimation for total intensity.

VI. CONCLUSION

A. SUMMARY OF FINDINGS

The work in this thesis involved two distinct aspects. First, the MUSTANG instrument was calibrated in preparation for the March 1994 launch from Poker Flats, Alaska. This calibration included a wavelength and a sensitivity calibration. The wavelength calibration fit a second degree polynomial to the wavelength versus pixel plot of the platinum and mercury lamp. This polynomial is used to determine the wavelength of each pixel in the image sensor. The sensitivity calibration calculated the calibration curve needed to convert the instrument output to an absolute intensity in Rayleigh's/Angstrom. This calibration also used two lamps of known output and required determining the reflectivity of the reflecting screen prior to calculating the final curve. The instrument was launched on March 10, 1994 and post-flight tests indicated that no significant change occurred in the calibration as a result of the rocket launch.

The second area of research was the estimation of the temperature profile from the NO $\gamma(0,1)$ and VK(0,5) bands, and the determination of the intensity profile of the OII 2470 Å multiplet. Data from the downleg of the March 1992

rocket launch from the White Sands Missile Range in New Mexico consisted of 42 records ranging in altitude from 115 km to 320 km. By fitting synthetically generated spectra for NO $\gamma(0,1)$ and N_2 VK(0,5) to the actual data, the contribution from these two emissions to the 2470 Å feature could be estimated and subtracted out. The remaining intensity is attributed to the OII 2470 Å emission and was fit with a synthetically generated spectrum similar to the procedure above. The constants used to fit the synthetic data to the actual data were then used to estimate the nitric oxide column density, the N_2 VK(0,5) intensity profile, the OII 2470 Å intensity profile and the temperature profile. These results will now be used as inputs to other models to infer the electron density profile for 115 km to 320 km.

B. RECOMMENDATION FOR FURTHER RESEARCH

During the calibration a 'hot spot' was discovered. Further research into the cause of this 'hot spot' and the effect it has on the output of the instrument would be beneficial.

APPENDIX

The instrument gain, Γ, in decimal units per photon per second is the product of the various efficiencies and transfer functions of the individual components of the instrument. In order to derive this quantity the following definitions are needed:

P -photon flux $\left(\frac{ph}{s * \mathring{A}}\right)$ received at the entrance slit over a one-Å wide wavelength bin

η_1 -quantum efficiency (el/ph) of the photo-cathode;

Γ_{mcp} -gain (el/el) of the microchannel plates;

η_2 -efficiency (ph/el) of the phosphor screen;

η_3 -quantum efficiency (el/ph) of the photo diode;

τ -integration time of photodiode (sec);

g_1 -transfer function (V/el) of the image detector amplifier;

g_2 -transfer function (decimal units/V) of the analog-to-digital conversion;

B_w -bandwidth of each pixel (Å/pixel).

Over one integration time, the output from a photodiode (W_{pd}) will be:

$$W_{pd} = P(\eta_1 \Gamma_{mcp} \eta_2 \eta_3 \tau) \qquad \text{(A-1)}$$

in electrons per Angstrom.

During this same period of time, the instrument output will be:

$$D = W_{pd}(g_1 g_2) B_w . \qquad \text{(A-2)}$$

Substitute Equation (A-1) into Equation (A-2), and rearranging terms gives:

$$D = P(g_1 g_2 \eta_1 \Gamma_{mcp} \eta_2 \eta_3 \tau) B_w . \qquad \text{(A-3)}$$

Therefore, the overall MUSTANG instrument gain, Γ, may be defined as:

$$\Gamma \equiv (g_1 g_2 \eta_1 \Gamma_{mcp} \eta_2 \eta_3 \tau) . \qquad \text{(A-4)}$$

LIST OF REFERENCES

Anderson, C.K., *A Calibration of the Naval Postgraduate School Middle Ultraviolet Spectrograph and an Analysis of the OII 2470 Å and OI 2972 Å emissions Obtained From Mid-Latitude Rocket Observations*, Master's Thesis, Naval Postgraduate School, Monterey, Ca., Sept. 1990.

Bosserman, James L., *Analysis of Thermospheric Dayglow Spectra from the Spacelab 1 Shuttle Mission*, Master's Thesis, Naval Postgraduate School, Monterey, Ca., Dec. 1989.

Chase, B.E., *A Calibration of the Naval Postgraduate School Middle Ultraviolet Spectrograph (MUSTANG)*, Master's Thesis, Naval Postgraduate School, Monterey, Ca., Dec. 1992.

Cleary, David D., "Daytime High-Latitude Rocket Observations of the NO γ, δ, ε, Bands", *Journal of Geophysical Research*, v.91, p.11337, 1986.

Danczyk, Gary M., *Identification of Thermospheric Dayglow Emissions for the MUSTANG Experiment*, Master's Thesis, Naval Postgraduate School, Monterey, Ca., Dec. 1989.

The Joint Chiefs of Staff Memorandum MJCS Serial 154-86 to Undersecretary of Defense (Research and Engineering), Subject: *Military Requirements for Defense Environmental Satellites*, 01 Aug. 1986.

INITIAL DISTRIBUTION LIST

1.	Defense Technical Information Center Cameron Station Alexandria, Virginia 22304-6145	2
2.	Library, Code 52 Naval Postgraduate School Monterey, California 93943-5002	2
3.	Dr. W.B. Colson, Chairman PH Physics Department Naval Postgraduate School Monterey, California 93943-5002	1
4.	Dr. D.D. Cleary Physics Department, PH-CL Naval Postgraduate School Monterey, California 93943-5002	3
5.	Dr. S. Gnanalingam Physics Department, PH-GM Naval Postgraduate School Monterey, California 93943-5002	1
6.	Lt. Hewitt M. Hymas 3415 South 8525 West Magna, Utah 84044	2

DUDLEY KNOX LIBRARY
NAVAL POSTGRADUATE SCHOOL
MONTEREY CA 93943-5101

DUDLEY KNOX LIBRARY
3 2768 00307291 9

3 2768 00307291 9